UiT
THE ARCTIC UNIVERSITY OF NORWAY

Department of Earth Sciences

Reconstructing the Holocene: Benthic Foraminifera as a proxy for the paleoceonography of the Nordic Seas

—

May Lizabeth Baker

Master's thesis in Marine Geology and Geophysics, August 2017

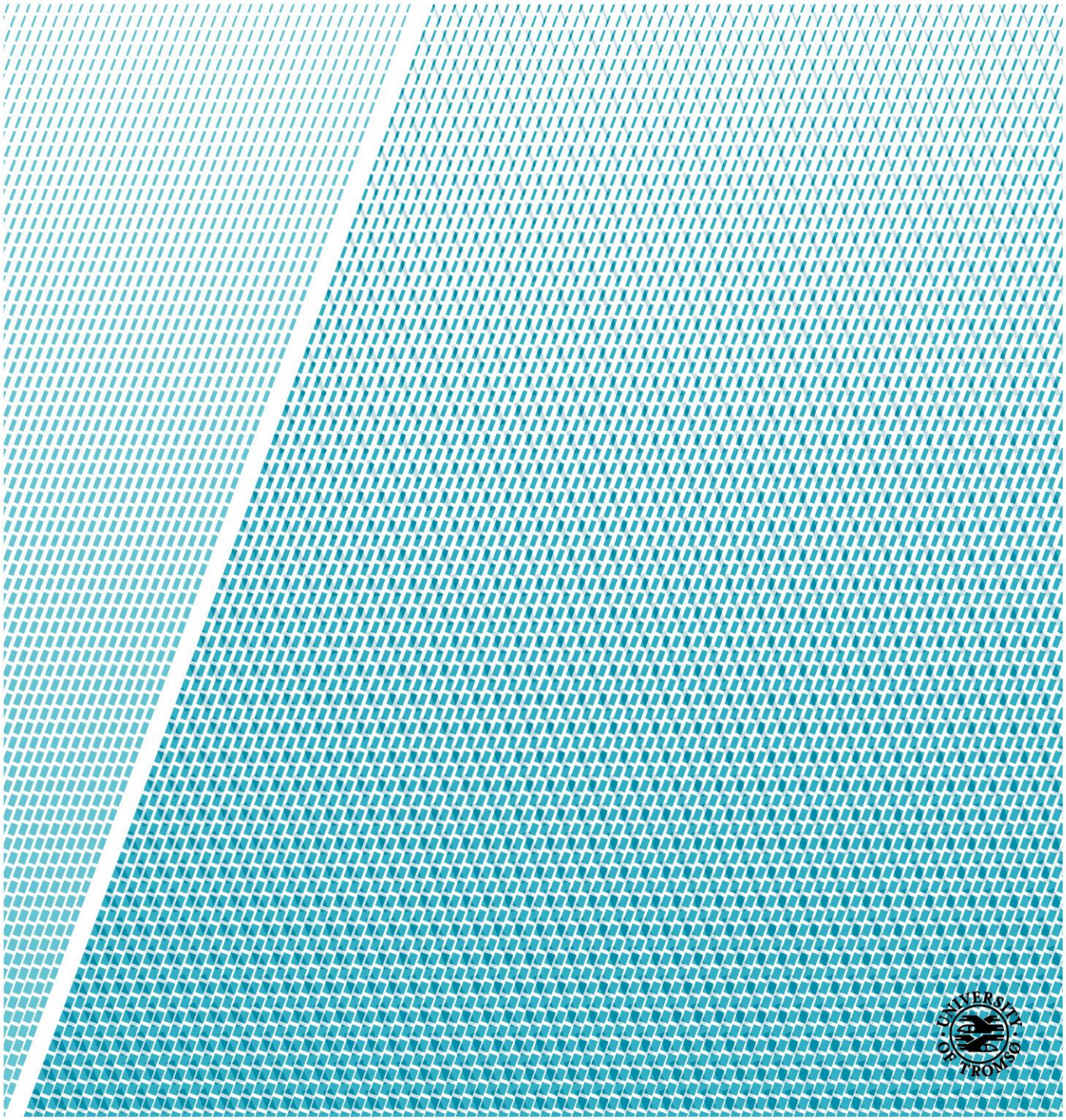

Acknowledgements

First, I would like to thank Tine Rasmussen my supervisor, for her help and guidance during this project. Thank you also to both my co-supervisors Kasia Zamelczyk and Juho Junttila. To Kasia for the kind use of her data sets and to Juho for guiding me in the lab and through endless excel formulas.

My lab work would could not have been completed without help from the laboratory staff, Trine, Ingvild, and especially Karina who has been a smiling presence every day.

To my friends, in the UK and here in Norway. The Core Four, Beth, Phoebe and Liv.

To my partner in crime Will, for blowing up my phone, endless ranting and for last minute pick and mix deliveries.

Last but most importantly, a shout out to my family. Wherever I am I always feel loved, and that is priceless.

May Lizabeth Baker

July 2017

Abstract

The benthic foraminifera of two marine sediment cores were studied as a proxy for paleoenvironment reconstructions throughout the Late to Early Holocene. The two cores were sampled in different localities to allow a spatial comparison of changing environments in the Nordic Seas and sampled for benthic foraminiferal assemblages, grain size, IRD, sortable silts and benthic foraminifera isotopes. While attempts at correlation were made, differing sedimentation rates made this difficult. A cold period spanning ~1000 years can be seen in both sediment records, attributed to the Dark Ages Cold Period. Benthic assemblages and isotope records show only vague similarities throughout the Late Holocene, suggesting that the core environments were subject to differing climatic influences due to their different localities, with only large scale climatic events effecting both areas equally.

Table of Contents

Chapter 1 - Introduction

1.1 Objectives

The objectives of this study are to reconstruct and compare the changing paleoclimate and paleoceanography of two sediment cores, HH13-103MC and HH12-1206BC, using benthic foraminifera and sediment properties as proxies for the investigation into their environments. The two cores were taken from different locations within the Nordic Seas, for a spatial comparison of water masses and bottom sediment environments.

1.2 Paleoceanography and Paleoclimate

In this thesis, both paleoceanography and paleoclimate will be discussed, and therefore it is important that they be properly defined.

Paleoceanography can be defined as the multidisciplinary scientific study of the changes within the oceans throughout history. It uses aspects of geology, glaciology, biology and chemistry to help recreate paleo-oceans. The factors involved in these reconstructions are known as "proxies". Proxies are classified as the indirect measurement of past climate or environmental change using preserved characteristics that stand in for direct measurements (Schneider, 2015). Example proxies include microfossils, ice cores, tree rings, and corals.

Ocean currents can have a large impact on climate through their changing directions and temperatures, and therefore paleoceanography is closely linked to the study of paleoclimate. Paleoclimate is the study of past climatic conditions and how present day environments came to be. Through the use of proxies, similar to that of paleoceanography, models of climatic changes throughout history can be made.

Following the principle that "the past is the key to the future", studying and understanding previous climate and ocean changes can help to understand how modern environments may also change and develop.

1.3 Study Areas

The first core discussed in this section is HH12-1206BC, taken from the Storfjorden Fan, to the South West of Svalbard. Storfjorden Fan is located at the front of the Storfjorden Trough, which extends from the mouth of Storfjord to the Svalbard shelf edge. Sedimentation within the fan consists of debris flows during glacial periods, and hemipelagic sedimentation during intergalcials. (Rasmussen and Thomsen, 2014)

The core site environment is heavily influenced by the warm West Spitzbergen Current (WSC). The WSC is a branch of the Norwegian-Atlantic Current, which in turn is a continuation of the North Atlantic Current (NAC), bringing warm and saline waters from the Atlantic equator. All of these currents form part of global thermohaline circulation, which is driven by differences in water temperature and salinity. It is this system which brings warm Atlantic surface waters to the Nordic Seas and along the western Svalbard shelf. Without this, environmental conditions in Arctic Norway and Svalbard would be much colder than they are presently. As the WSC continues northwards it cools and becomes denser. This increasing density causes the WSC to sink below less dense colder and less saline polar waters. The meeting of warm Atlantic and cold Arctic waters is called the Arctic Front (Schepper et al., 2015).

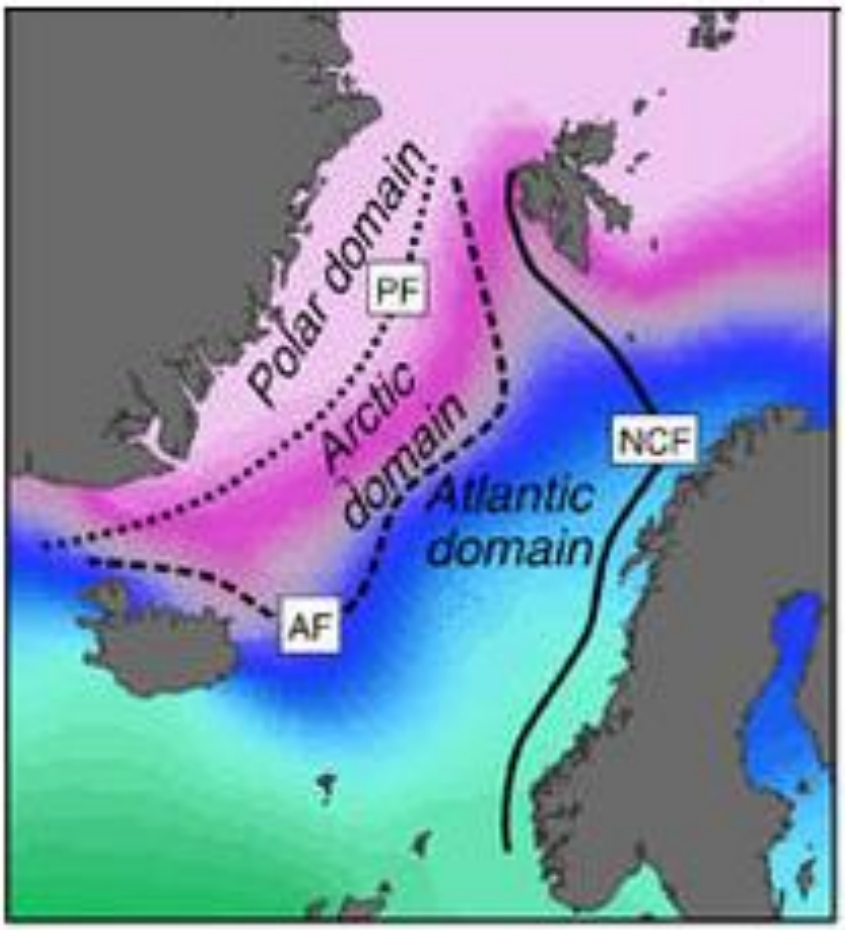

Figure 1: Division of the Nordic Seas (made up of the Norwegian Sea, Iceland Sea and Greenland Sea) by the Polar Front (PF) and Arctic Front (AF) based on modern surface temperatures. The Norwegian Continental Front (NCF) from south to north along the Norwegian Continental Shelf.

Image adapted from Schepper et al., 2015.

The second core, HH13-103MC, was sampled further south, to the south east of Jan Mayen. Jan Mayen is a small volcanic island within the Norwegian-Greenland Sea. It is located on the Jan Mayen Ridge microcontinent, which formed after the Atlantic rifting zone relocated from the no longer active Ægir Ridge, to the active Kolbeinsey Ridge (Gjerløw et al., 2016).

Situated on Jan Mayen island is the active stratovolcano Beerenberg which has several recorded eruptions since the discovery of the island, the earliest known eruption being in 1732 AD. Gjerløw et al., 2016 show that while there are previously unrecorded eruptions from Jan Mayen during the Holocene, volcanism on Jan Mayen is mild or strombolian in nature, and therefore there is little tephra dispersal over the surrounding area. Due to these eruptions, sediments are unlikely to reflect eruptions in their composition with only minor tephra layers found in sediment cores. The island is effected seasonally by surrounding pack ice during the winter which retreats in the summer.

The Norwegian-Greenland Sea is predominantly made up of two main basins, the Greenland Basin to the west of Jan Mayen, and the Norwegian Basin to the east. HH13-103MC is situated on the edge of the Norwegian Basin on the Jan Mayen ridge. As with core HH12-1206BC, HH13-103MC is also affected by the NAC which branches at approximately 60^{o}N as it flows through the Denmark Strait, across the Iceland-Faroe Ridge and through the Faroe-Shetland channel. Here, a branch flows towards Jan Mayen bringing warm saline waters to the Norwegian Basin and into the Greenland Basin (Meinke, Rudels and Friedrich, 1997).

The Greenland Basin is primarily influenced by cold water flowing from the East Greenland Current (EGC). The EGC flows south from polar regions and along the East Greenland continental margin, bringing cold fresh polar waters from the Arctic and forming the Polar Front. A branch of the EGC flows west from the East Greenland continental margin and into the Norwegian Basin. South of Jan Mayen, there is mixing of the EGC and NAC in the cyclonic Greenland Gyre (Aagaard, Swift and Carmack, 1985).

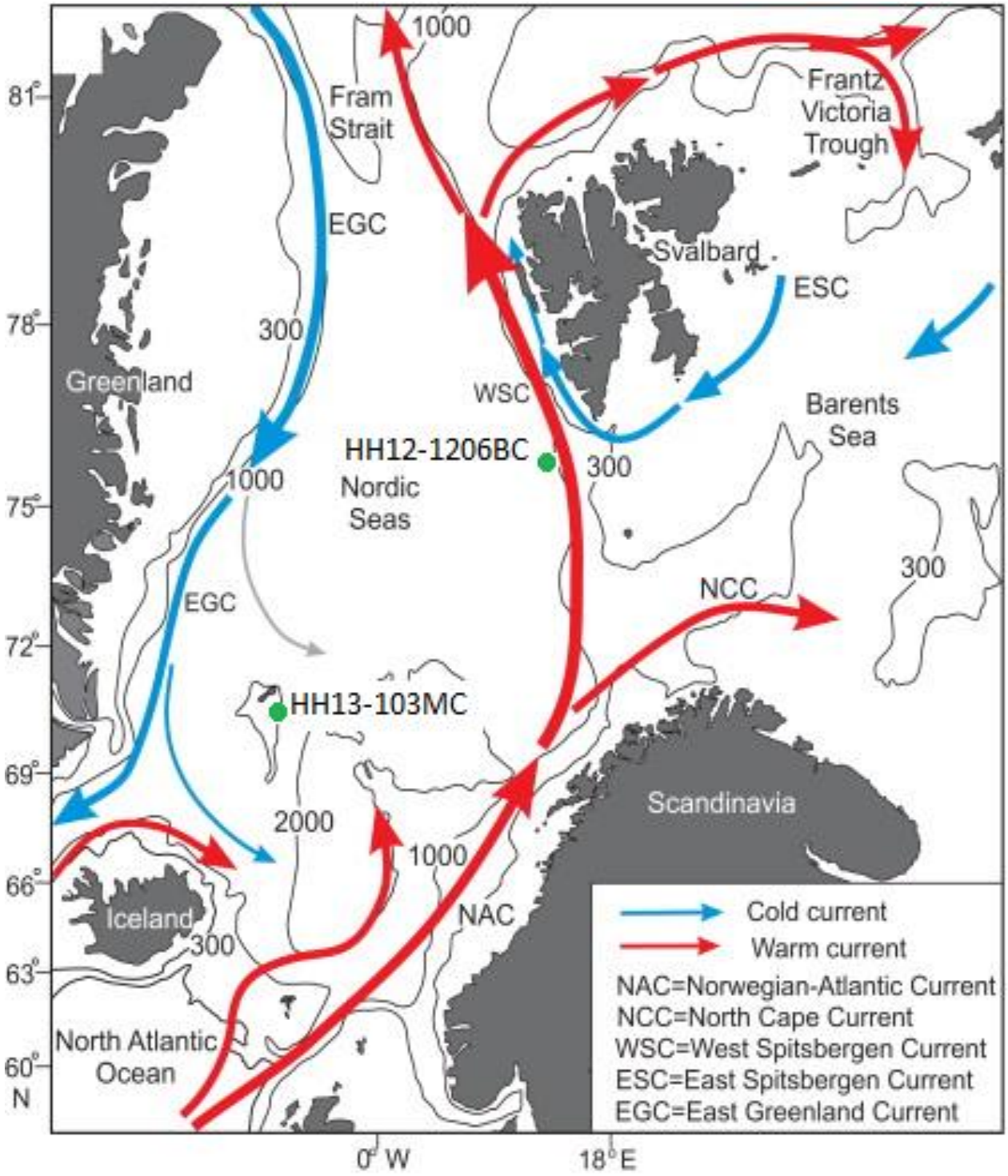

Figure 2: Showing the major ocean currents of the Barents and Nordic Seas. Study core locations are shown in green. Modified from Rasmussen et al., 2014.

1.4 Evolution of Holocene Paleoceanography and Paleoclimate

The Holocene is the inter-glacial time period from 11,700 YrsBP to present within the geological time scale and corresponds with marine isotope stage one (MIS1). Although there is no formal division of the Holocene, it can be divided into three sub-units consisting of the early Holocene 11,700-8,200 YrsBP, the Mid-Holocene of 8,200-4,200 YrsBP and the late Holocene from 4,200 YrsBP to present (Walker et al., 2012). The changing paleoceanography and paleoclimate of these units are discussed below.

1.4.1 The Early Holocene 11.7-8.2 KaBP

During the earliest Holocene from 11.7-9.6KaBP the Svalbard shelf was dominated by cold polar waters and icebergs which supplied fresh melt water to the surface waters. The bottom waters however were much warmer and temperatures during this time were the highest for bottom waters throughout the Holocene (Rasmussen et al., 2014). A short but distinct period of cooling known as the Preboreal Oscillation (PBO) at around 11-11.3 KaBP reduced bottom water temperatures and salinity (Aagaard-Sørensen et al., 2013). The PBO has been linked to an increase of deglacial meltwater flux and reduced heat transport to the Nordic Seas by the NAC (Fisher et al., 2002). After the PBO there was an increasing flow of Atlantic water at greater depths while polar waters still dominated the surface, creating a stratified water column and limited biological productivity. Seasonal sea ice cover or a close proximity to the Arctic front was at ~74^{o}N along the western Barents Sea margin (Groot, 2013).

A decrease in Ice Rafted Debris (IRD) and an increase of planktic foraminifera flux from 10 Ka BP suggests an increasing temperature of surface waters and an increasing productivity as Atlantic waters began to have a stronger influence on surface waters (Rasmussen at al., 2007). This coincided with an increase of ventilation within the water column and the transport of enriched organic material to the sea floor (Aagaard-Sørensen., 2010). As the Atlantic water began to have more influence on surface waters it is likely that the Arctic front moved northwards and eastwards (Risebrobakken et al., 2010). However while the surface waters warmed, the bottom waters saw a gradual cooling trend which could be attributed to a cooling of the incoming Atlantic waters (Risebrobakken et al., 2011). This cooling continued into the Mid-Holocene.

1.4.2 The Mid-Holocene 8.2-4.2 Ka BP

In the Mid-Holocene subsurface water temperatures reached a thermal maximum, followed by a general cooling from 6000Yrs BP, while bottom waters were colder than during the Early Holocene. This cooling of bottom water temperatures can be attributed to a cooling of the NAC due to a

reduced insulation effect in the Northern Hemisphere from reduced ice cover (Groot, 2013; Andersson et al., 2010).

A period of cooling is recorded across the North and Barents Seas between 9-8KaBP and again at 6.5KaBP. Southern areas in the North Sea and Nordic Sea recorded an earlier onset of these cooling periods and a longer duration than the northern Barents Sea (Hald et al., 2007), meaning spatial differences of climate across the Nordic Seas. Ice rafting shows an increase as land ice starts to advance again from 7KaBP, while bottom water temperatures decreased on the slope following the cooling trend shown on the shelf (Rasmussen et al., 2014).

1.4.3 The Late Holocene 4,2KaBP-Present

The cooling trend of the Mid-Holocene continued into the Late Holocene, with a shift from warm Atlantic to colder Polar waters dominating the surface waters. This is reflected in a significant decrease in the numbers of planktic foraminifera and an increase in IRD flux to levels similar to that of the Early Holocene (Aagaard-Sørensen et al., 2013; Andersen et al., 2004; Rasmussen et al., 2014).

A series of cooling and warming periods is seen throughout the Late Holocene, known as the Neoglacial (SOURCE), with advancing and retreating glaciers seen around the globe. The most well known of these fluctuations are the Dark Ages Cold Period (DACP) from 400-800AD, the Medieval Warm Period (MWP) from 950-1250AD, and the Little Ice Age (LIA) from 1400-1700AD (Mann et al., 2009).

Chapter 2 - The Use of Proxies

2.1 Benthic Foraminifera

"Foraminiferida are an order of single-celled protists that live either on the sea floor or amongst the marine plankton" Loeblich and Tappan, 1987

This study focuses on benthic foraminifera, which are micro-organisms living within or on the sea floor. They which can be classified into one of two positions of life; either epifaunal or infaunal. Epifaunal species live on the surface of the substrate, while infaunal species live within the sediment. Benthic foraminifera produce a shell, or test, made either from calcium carbonate ($CaCO_3$) which is mineralised from the ocean, or the test can be agglutinated. Agglutinated tests are constructed from organic or mineral particles on the sea floor which the foraminifera binds together using an organic or calcareous cement (Braisier, 1980).

Microfossils are a good proxy choice for environmental reconstructions as they are often well preserved after deposition, and can be abundant even in small sediment samples. They are widespread, and can be found in many variable environments. Furthermore, foraminifera in particular can be defined as bio-indicators; "a key group or species characterised by fast turnover rates and specific habitats" (Dijkstra et al., 2013). Foraminifera have a short life span, ranging from weeks to months depending upon the species, meaning their populations and assemblages act as indicators of environmental change when compared to other macro-fauna (Murray, 2006). Furthermore, foraminifera are sensitive to many environmental factors such as temperature, food availability, oxygen, substrate, salinity, light, sedimentation rates and currents. Benthic foraminifera especially can be sensitive to changes to their habitat, and there is a wide variety of species that are able to tolerate different levels of environmental stress.

Image 1: Dorsal and ventral views of example benthic foraminifera species.

A: *Cibicides wuellerstorfi*

B: *Hoeglundina elegans*

2.1.1 Species Assemblages and Diversity

Species of benthic foraminifera can be categorised by their response to environmental stress, and this further helps to determine changes of environmental conditions within their habitats. Faunal assemblages that have been impacted by environmental stress show lower species diversity, lower density, deformation and a higher number of opportunistic species compared to sensitive species (Alve and Bernhard, 1995).

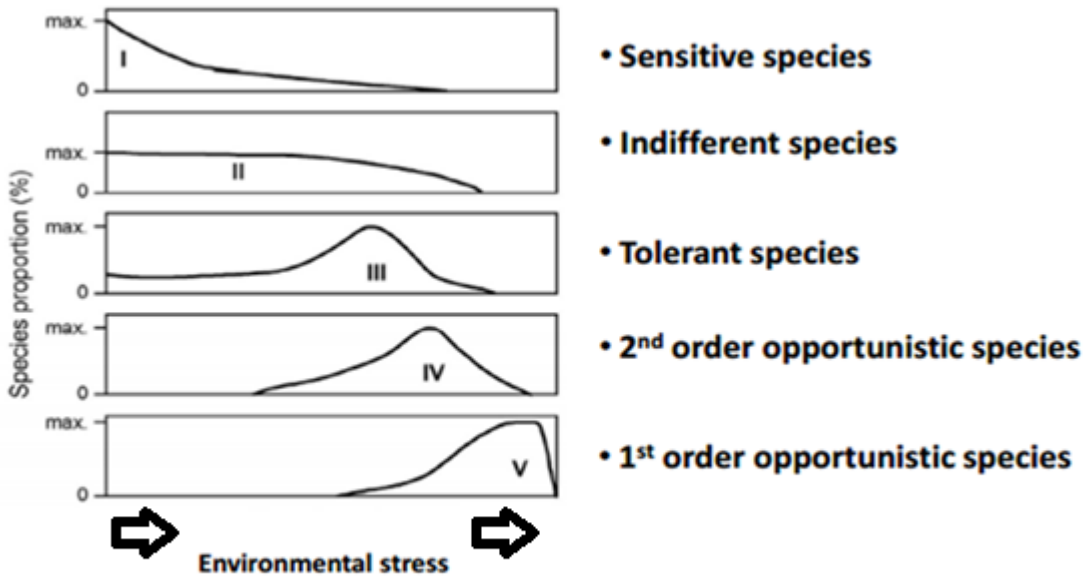

Figure 3: The proportion of benthic foraminifera in response to environmental stress.

2.1.2 Oxygen and Carbon Isotopes

During the formation of their carbonate shells, foraminifera preserve the isotope ratio of Carbon, Calcium and Oxygen, which is then preserved when they die. Using the ratios of O^{18}/O^{16} and C^{13}/C^{12} the palaeo-salinity and palaeo-temperature of the environment can be established.

Oxygen and carbon consist of stable isotopes, the ratio of which can change due to temperature and age. Oxygen is made up of O^{16}, O^{17}, and O^{18}. Water molecules can be formed using either the "light" form of O^{16} or the "heavy" form of O^{18}. O^{18} takes more energy to evaporate and will condense before its lighter counterpart of O^{16}. This preferential evaporation is temperature controlled, therefore during periods of colder temperatures δO^{18} (the ratio of O^{18}/O^{16}) will be higher, as the light O^{16} will be removed from the ocean surface first. This ratio of isotopes is recorded by foraminifera during the building of their tests, as they mineralise calcium carbonate from the sea water and can be

measured using a mass spectrometer. The isotope levels produced can then be used as an indicator for temperature and salinity of the water in which the organism lived.

Carbon is found in two isotopes of C^{12} and C^{13}. The δC^{13} (ratio of C^{13}/C^{12}) values found in the tests of benthic foraminifera reflects the values of C^{13} of dissolved inorganic carbon in water masses, and therefore δC^{13} can be used as an indicator of water mass ventilation and deep sea circulation (Ishimura et al., 2012; Mackensen and Bickert, 1999).

The bottom water temperatures and salinities can be reconstructed using transfer functions. Transfer functions are defined as "empirical statistical models that describe the relationship between organisms occurring at present and their environment" (Husum and Hald, 2012). This can then be used to provide quantitative data for palaeoclimate reconstruction estimates, assuming that the relationship between the species and environmental factor has not changed.

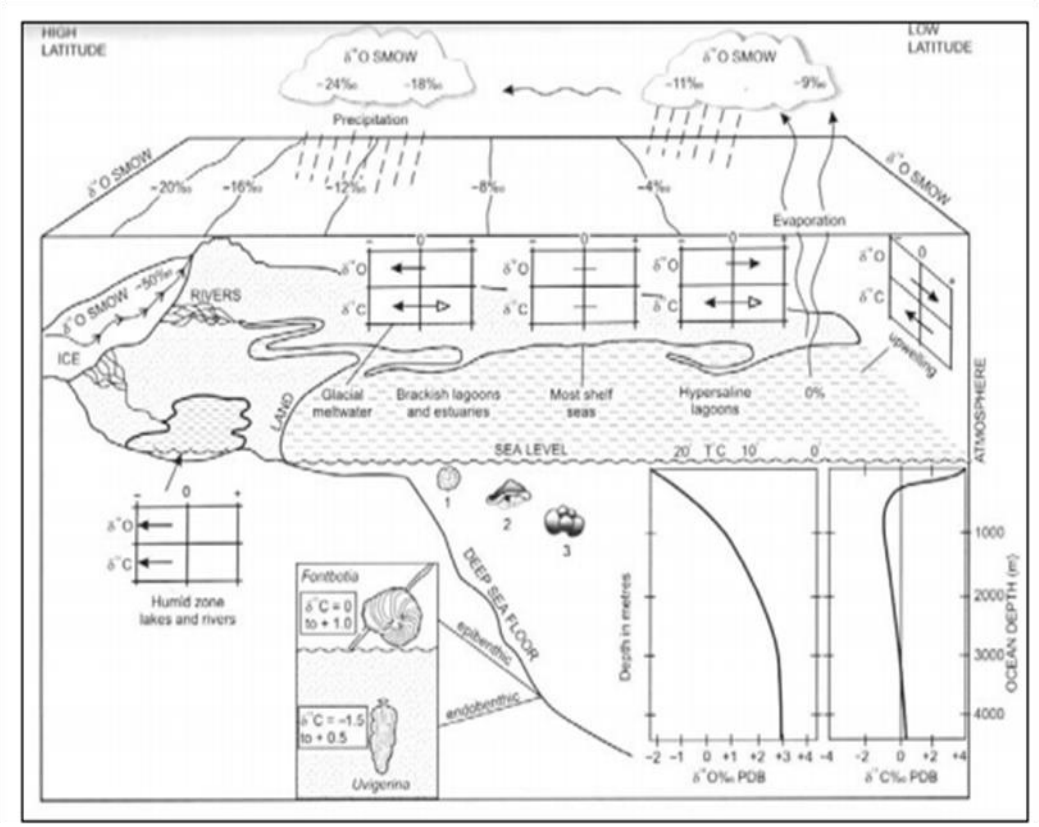

Figure 4: The changing ratios of oxygen and carbon isotopes found in foraminifera tests in response to depth and salinity. Black arrows show typical isotope trends as conditions become more extreme. (Hofmann).

2.2 Alternative Proxies for Paleoclimate and Paleoceanography reconstuctions

2.2.1 Ice Rafted Debris (IRD)

Ice Rafted Debris (IRD) is found in areas affected by sea ice or icebergs. Coarse grained sediments can be trapped in the ice, which are then transported by the ice and released as the ice melts. This sediment can be used as a proxy to help reconstruct ice drifts and paleoclimate (Moros et al., 2006).

2.2.2 Sortable Silts

Changes in sea floor flow rates and bottom currents can be investigated using sortable silts. The "sortable" referring to the fraction size of sediments which are most often affected by changes in flow rates. This fraction is set at 10-63µm, and can be measured to use as a proxy for palaeocurrent. Material that is over 63µm has been determined to be too heavy to be transported via deep sea currents, and therefore is presumed to be deposited by ice rafting (Hass, 2002). This correction and the equations used in this process is discussed further in section 3.5.

As flow decreases finer grained sediments are able to settle out of suspension, and with stronger currents cause a coarsening of sediments as finer materials remain in suspension, thereby recording the current flow in the sediment record (Jessen and Rasmussen, 2015; McCave et al., 1995).

Chapter 3 – Methods and Materials

3.1 Sediment Core Collection

Two sediment cores were collected for this study. The first, HH12-1206BC from the Storfjorden Fan and the second, HH13-103MC from South East of Jan Mayen. Both cores were taken from the R/V Helmer Hansen, in 2012 and 2013 respectively. Along with each core extraction, CTD (conductivity, temperature and density) measurements were also taken. Details of the cores are given below.

Core Name	Core Type	Date	Time	Location	Co-ordinates	Depth (m)	Core Length	Additional Information
HH12-1206BC	Box Core	24/10/2012	20:22	Storfjorden Fan	76.23.7222'N 012.58.199'E	1520	33cm	Site of JM03-373P
HH13-103MC	Multi Core	04/07/2013	23:50	Southeast Jan Mayen	70.45.545'N 005.15.422'W	2374	54cm	3 tubes of 5 retrieved.

Table 1: Drilling sites and collection methods used for the two cores discussed in this study.

HH12-102BC was taken as a sub-core within a box core. The box corer is lowered from the side of the R/V Helmer Hansen through a series of trawl winches to the seafloor, where a singular large sample of sediment is collected and bought to the surface. Once onboard, a plastic tube of 15cm in diameter is inserted into the collected sediment, to create a vertical sediment sub sample. The sub-core is then removed from the box corer and sealed. This method can cause some sediment contamination from drag as the tube casing is inserted into the sediment but this effect is minimal.

HH13-103MC was sampled using a multi corer. The multi corer consists of a metal frame with attachments for up to six plastic tubes for sediment collection. As with the box corer, the multi corer is lowered from the R/V Helmer Hansen, to the sea floor. The weight of the corer means that the tubes are inserted into the sediment. Core catchers placed at the bottom of each tube ensure that sediment which enters the tube is unable to fall out again. Once back on board the ship, the sediment catcher is removed from the bottom of the tube, and plastic caps seal the tube at both ends to ensure containment of the sediment. It is necessary to transport and store the tubes containing the sediment cores in a vertical position so that the stratigraphy of the sediment is preserved.

Core HH13-103MC was opened and subsampled in the geology laboratory within the department of Earth Sciences at UiT:The Arctic University of Tromsø. Subsampling was completed using a core extruder. The sediment core was placed on top of the extruder, and slowly pushed down. As the

sediment was pushed up and out of the top of the tube, it was measured in 1cm intervals and removed using metal spatulas. The sediment was then placed in labelled plastic bags and weighed to record the wet weight of the sediment before drying. A total of 51 samples were collected from the core.

Core HH12-1206BC was opened and sampled every 0.5cm by Kasia Zamelczyk at UiT. Data sets of grain size analysis and Carbon dating were then provided for this study, having been collected using the same methods described below for core HH13-103MC. 60 sediment samples from 31cm of core were also provided for benthic foraminifera species analysis and isotopes. It was found that two samples had become lost in transit. The data for these samples has therefore been omitted.

3.2 Foraminiferal Analysis

To allow foraminiferal analysis, the samples collected were placed into a freeze dryer to remove water. The freeze drying process involves the vaporisation of water which is less destructive for the preservation of foraminifera. After drying the samples were weighed a second time to record the dry weight. Using this data it was then possible to calculate the water content of each sample.

Half of each sample was then wet sieved using four stacked sieves at 1mm, 500µm, 100µm and 63µm size fractions. Sediment remaining in each sieve was placed on labelled filter paper and dried within a warm oven at 40^{o}C for at least 24hours. After the samples were fully dry, they were weighed and transferred to labelled glass dram vials for storage.

To create a benthic foraminifera faunal distribution, the samples were dry picked from the 100-500µm size fraction. A small amount of the sample was spread evenly across a counting tray, and the remaining sample weighed to know the weight of sediment within the tray. Benthic foraminifera were then counted and collected in a separate labelled microscope slide. For every sample ≥300 foraminifera were counted. For some samples this number was not possible so instead all benthic foraminifera within the sample were picked. It is possible that some foraminifera were overlooked during picking. Each specimen was then identified, if possible to species level. Species identification was completed using the World Register of Marine Species (WoRMS) database (WoRMS Editorial Board, 2017).

Using this data, the relative abundance of each species in a sample was calculated as the percentage of the species in relation to all other counted specimens in the sample.

The percentage abundance of each species identified was calculated using the formula below:

$$Percentage\ Abundance = \frac{Nunber\ of\ specimens\ of\ a\ given\ species}{Total\ number\ of\ benthic\ formaminifera\ in\ sample} * 100$$

Total benthic foraminiferal flux was calculated using the formula below:

$$MAR = LSR * Dry\ Bulk\ Density\ (g/cm^3)$$

$$Foraminiferal\ Flux = Foraminifera\ concentration * MAR$$

Where MAR = Mass Accumulation Rate ($g/cm^3/Ka$), LSR = Linear Sedimentation Rate

Diversity of each sediment core was also determined using the Shannon Index (Shannon, 1948). This was completed using the PAST software, version 2.17 (Hammer et al., 2001). The Shannon Diversity Index is a measure of heterogeneity diversity, meaning that it takes into account not only the number of species found but also the distribution of individuals among the species (Gray, 2000).

3.3 Carbon and Oxygen Isotope Analysis

For both cores the species *C. wuellerstorfi* was chosen for stable isotope analysis due to its relatively larger size and abundance throughout each core. *C. wuellerstorfi* was also chosen as it forms its test close to the equilibrium due to its epifaunal nature. Living on elevated surfaces it is not influenced by the pore water chemistry within the substrate and therefore it is the best measure of bottom water C^{13} (Gupta, 2007). Around 5-10 specimens of *C. wuellerstorfi* were picked from each sample depending on abundance, size and preservation quality. They were then placed directly in labelled glass tubes. It was then decided that due to the large nature of the *C. wuellersotrfi* these samples could be split, so that each sample could be run twice. The samples were analysed at the University of Tromsø, Department of Earth Sciences, using a Thermo-Fisher MAT253 IRMS with Gasbench II Mass Spectrometer.

3.4 AMS Radiocarbon Dating

Accelerator Mass Spectrometry (AMS) Radiocarbon dating works by measuring levels of the radioactive isotope C^{14} relative to stable C^{12} within the atmosphere. As C^{14} is unstable, it decays over time. This process has a constant decay rate of approximately 5730 ± 30years. During its lifetime an organism uptakes C^{14} from the atmosphere, so that C^{14} is constant in both the atmosphere and the organism. After death the C^{14} left in the body of the organism will start to decay. Therefore it is possible to measure and compare C^{14} levels within a deceased organism and the present atmosphere. This difference gives us AMS Radiocarbon dating. Using this process it is possible to date up to 50,000yrs before present (BP).

However, due to changes in C^{14} values in the atmosphere over time, C^{14} dating does not correlate directly with calendar years. There is also a delay between atmospheric CO_2 entering the oceans at the sea surface-atmosphere boundary, and the dilution effect caused by the mixing of surface waters containing present C^{14} values and up-welled older deep waters in which the C^{14} has already begun to decay. Marine organisms may take up C^{14} which from these deep waters and therefore will test older than they are during AMS dating. This is called the Marine Reservoir Effect or R (Ascough, Cook and Dugmore, 2005). The average R of the ocean's surface is ~400years but this can vary spatially due to regional differences in water masses and currents (ΔR). Therefore AMS dates need to be corrected to compensate for this effect and to correlate to calendar years.

Calibration of the AMS radiocarbon dates obtained for this study was completed using the programme CALIB 7.0.4, which uses the MARINE 13 radiocarbon calibration curve (Reimer et al., 2013).

Due to nuclear testing since 1950 AD, the levels of C^{14} in the present day atmosphere are higher than would be naturally produced. Therefore AMS radiocarbon dating uses 1950 AD as present day.

After the counting of benthic foraminifera, three samples from core HH13-103MC were decided upon for dating. This decision was based on the number and diversity of foraminifera, and having samples spaced equally within the core to be able to later create an age model. From each of the three chosen samples, 8mg of *N.pachyderma* (sinistral), and 8mg of *C. wuellerstorfi* were picked and sent to the ^{14}CHRONO Centre, Queens University, Belfast, Northern Ireland. The samples were sent in labelled plastic vials, which were in turn packaged in bubble wrap and placed in a padded envelope to ensure a safe delivery. At the time of writing, only one AMS radiocarbon date has been received, therefore dating for core HH13-103MC was completed using core correlation. See section 4.3 for details.

Dating for core HH12-102BC had already been carried out through the same process. These correlated dates and an age model created by Kasia Zamelczyk were both provided for this study.

3.5 Grain Size Analysis

From the remaining un-sieved sediment of the freeze dried samples of core HH13-103MC, 2g was placed into labelled plastic test tubes, and covered with 20% Hydrochloric Acid (HCL). The tubes were left in a fume cupboard for 24 hours to remove calcareous material within the sediment. After this time the tubes were placed in a centrifuge for 4 minutes at 4000rpm. The HCL was then removed and distilled water was added. After the water was added the tube was shaken to ensure that all sediment was in suspension, and placed in the centrifuge again. This washing process with

the centrifuge and distilled water was repeated twice so as to completely neutralise any remaining acid in the sediment. After washing the samples were covered with Hydrogen Peroxide (H_2O_2) which removes any remaining organic material within the sediment. The tubes were covered with aluminium foil and placed in a heating bath at 80^OC for two hours to help catalyse the reaction. A small hole in the foil lids allowed gas to escape during the reaction process. The tubes were also closely monitored during their time in the heating bath as some reactions can become too strong. During strong reactions sediment may be expelled from the tube and lost. In these cases the tubes must be removed from the heating bath and allowed to cool and the reaction to diminish before being placed back in the heating bath.

After the 2 hours the samples were removed from the heating bath and were again centrifuged and washed three times with distilled water to neutralise the sediment. After washing the remaining sediment was flushed into labelled plastic cups using distilled water and placed to dry within a fume cupboard. All laboratory work while using HCL and H_2O_2 was carried out within the fume cupboards at the UiT Department of Earth Sciences for safety purposes.

When fully dried, 0.5g of sediment was left in the plastic cups and the rest removed and transferred to labelled plastic bags to be stored. 20ml of tap water was added to each of the plastic cups, which were then placed in an Edmund Bühler GmbH SM-30 universal shaker for a minimum of 24 hours to ensure the entirety of the dried sediment was in suspension before analysis. Two drops of Calgon solution was added to each sample to prevent flocculation of sediment before then being placed in an ultrasound bath for five minutes. Next the samples were poured through a 2mm sieve before they were then analysed using an LS13320 Laser Diffraction Particle Size Analyser (LDPSA). Each sample was analysed three times by the LDPSA to create an average measurement. The average was then inputted into the programme GRADISTAT v 8.0 to determine the percentage composition of each grain size fraction.

Grain sizes described are based on the Udden-Wentworth classification scale as shown in Figure 5.

3.6 Ice Rafted Debris (IRD)

Sediment collected after sieving was counted for IRD in the 500µm-1mm and >1mm fractions. The number of grains were counted for each fraction, and using this the number IRD per gram was calculated. During counting the number of light and dark mineral grains were also noted so that the percentage of dark to light could be calculated.

Grain Size		Descriptive term	
phi	mm		
		Very Large	Boulder
-10	1024		
		Large	
-9	512		
		Medium	
-8	256		
		Small	
-7	128		
		Very small	
-6	64		
		Very coarse	Gravel
-5	32		
		Coarse	
-4	16		
		Medium	
-3	8		
		Fine	
-2	4		
		Very fine	
-1	2		
		Very coarse	Sand
0	1		
	microns	Coarse	
1	500		
		Medium	
2	250		
		Fine	
3	125		
		Very fine	
4	63		
		Very coarse	Silt
5	31		
		Coarse	
6	16		
		Medium	
7	8		
		Fine	
8	4		
		Very fine	
9	2		
		Clay	

Figure 5: Scale size used in GRADISTAT v 8.0 programme, adapted from Udden (1914) and Wentworth (1922)

3.7 Sortable Silts Analysis

Results from the grain size analysis were also used to calculate the sortable silts of core HH13-103MC and changing bottom current strengths. To do this, data from the silt fraction 10µm-63µm was inputted into GRADISTAT v 8.0. The silt fraction based on the Udden-Wentworth classification is defined as 2µm-63µm, however particles may flocculate and therefore the minimum fraction was raised to prevent inclusion of these aggregates.

Due to the positioning of core HH13-103MC, it is possible that the sediment found within the core was influenced by icebergs and any IRD that they may deposit. This may include sediment within the silt fraction, which would affect the measured sortable silt analysis. Hass (2002) describes how the plotting of sand fraction (%) against the mean sortable silt (SS) can be used to test if the silt fraction has been influenced by ice rafting. If a positive correlation is found between the two then it is most likely that some of the silt fraction was ice rafted and the SS can then be corrected to account for this.

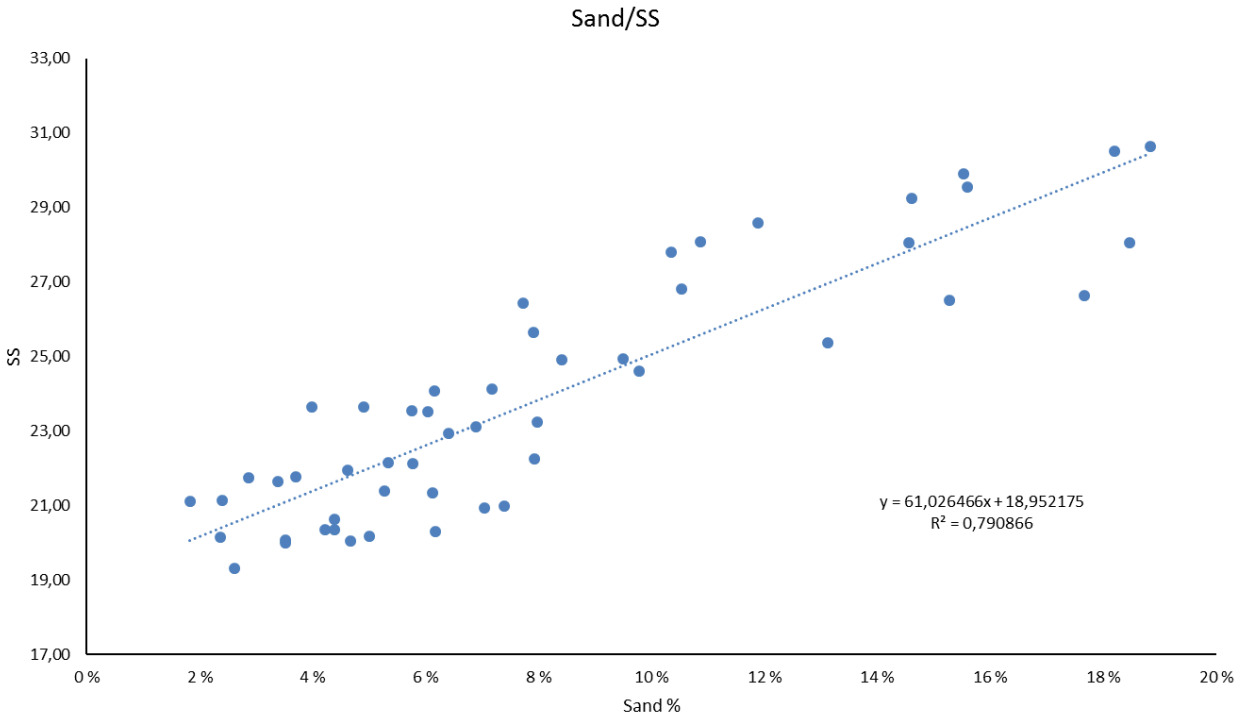

Figure 6: Scatter plot of % Sand against SS for core HH13-103MC. The positive correlation seen suggests influence of IRD on the silt fraction.

The correction of IRD influence on SS can be calculated using the following equation:

$$\Delta SS = SS - SS_{\text{pot}}$$

Where ΔSS is SS modified by current speed corrected for IRD influence, and SS_{pot} is the SS which has potentially been influenced by IRD. SS_{pot} can be calculated using the method from Hass (2002):

$$Y = 61.026466 * (x + 18.952175)$$

Where Y is SS_{pot} and x is sand %.

Chapter 5 - Results

5.1 Diversity Index

The diversity index of both cores were calculated according to the Shannon Diversity Index (Shannon, 1948). A higher value of the index (H) indicates a greater richness and evenness of the community. The diversity index of the two cores have been plotted against each other to allow comparison.

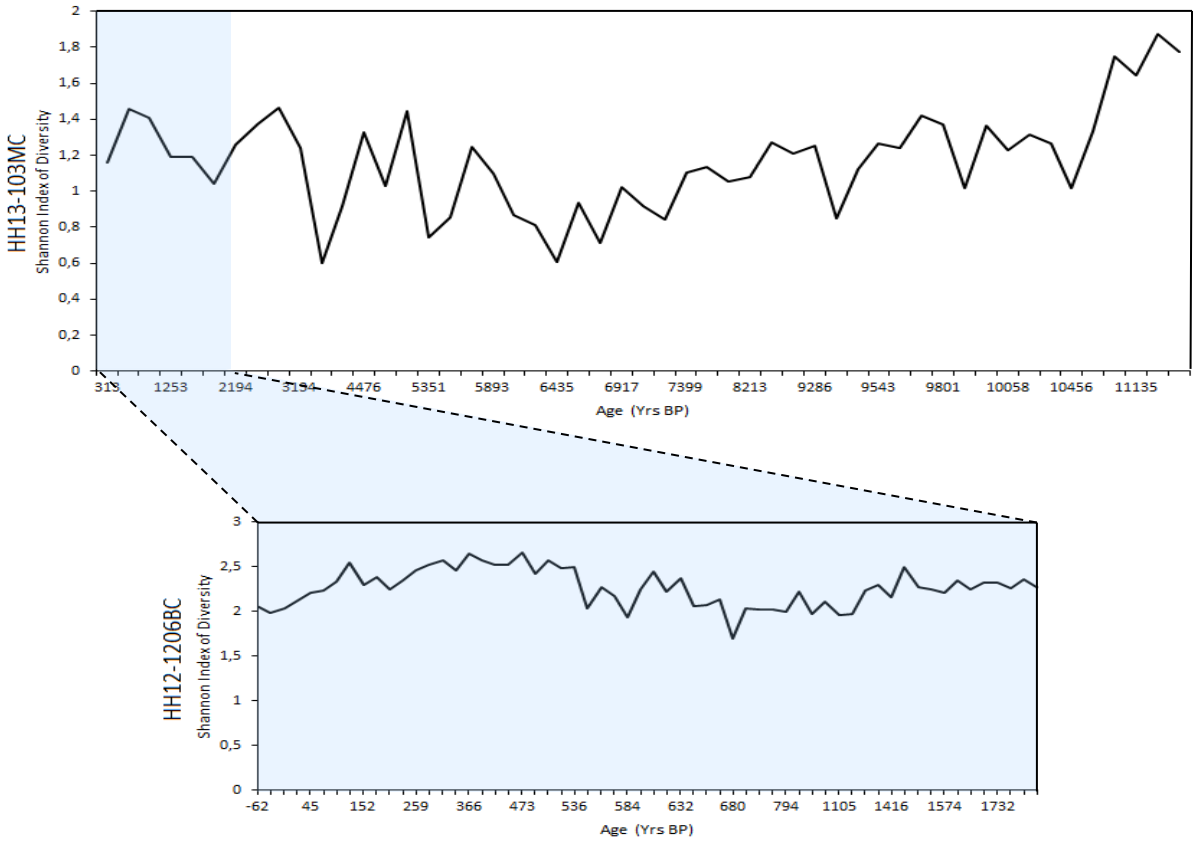

Figure 7: Calculated Shannon Diversity Index of sediment cores HH12-1206BC and HH13-103MC.

Core HH12-1206BC shows a significantly higher index of diversity (H) when compared to core HH13-103MC. As the two cores cover different time scales there is a lack of correlation between the two data sets. This could also be a result of the spatial differences between the two cores. Core HH13-103MC has a generally decreasing H, throughout the bottom of the core, which started to increase after 6435Yrs BP although there are significantly low levels seen at 5351Yrs BP and 3447Yrs BP.

Lows within core HH12-1206BC are seen at 692Yrs BP, 596Yrs BP and 560Yrs BP.

5.2 Benthic Foraminifera Assemblages

As discussed previously, benthic foraminifera can be used as a proxy for palaeoceanographic reconstructions using the changing species assemblages within the sediment due to the diverse range of species and the favoured environments of different species. This section will focus of the dominating species of benthic foraminifera found in the two study sediment cores.

5.2.1 HH13-103MC

A total of 28 species were identified from the sieved sediment samples from core HH13-103MC, within the size fraction 100-500µm. Below are described the dominating species identified.

***Cibicidoides weullerstorfi (*Schwager, 1866)**

Cibicides wuellerstorfi is an epifaunal species, living on the sea floor, and in many cases attaches to hard substrates between 3-7mm above the surface sediment (Lutz and Thiel, 1989). It is a suspension feeder, feeing on particles transported by bottom currents. It is a dominant species found in areas of North Atlantic Deep Water (NADW) and fluctuations in the abundance of this species can indicate temporal changes on the advection of NADW (Gupta, 2007).

Overall the specimen counts of *C. wuellersotfi* seem to be negatively correlated to Δ SS, with numbers decreasing as the current strength increases, particularly between 10-15, 27-33 and 42-48cm depth. However there are moments of a direct positive correlation at 9-10, 16-18, and 38cm respectively.

From 24cm numbers of *C. wuellerstorfi* decrease significantly throughout towards the bottom of the core, with only one large peak at 35cm, which corresponds to a decrease of *H. elegans* and *Globobulimina sp.*

***Islandiella norcrossi* (Cushman, 1933)**

Islandiella norcrossi is a shallow infaunal species which prefers to feed on fresh organic matter in fine grained sediments, and favours relatively high bottom water salinities. It is known as an indicator species for a higher organic nutrient content, an increased productivity and a close presence to the sea ice edge (Rasmussen et al., 2007) or glacial-distal faunas (Korsun and Hald, 2000).

Levels of *I. norcrossi* show both a negative and positive correlation to Δ SS, with a strong positive correlation seen at 11-14cm depth. However, at 16cm the number of *I. norcrossi* drops significantly,

disappearing from the sediment core completely at 26cm.Therefore it is possible that grain size is not a controlling factor for this species.

***Hoeglundina elegans* (d'Orbigny, 1826)**

Shallow infaunal or epifaunal, *H. elegans* is most often found on the lower shelf slope between 400-2000m and is associated with low organic flux rates (Gooday, 2003). In this core, *H. elegans* shows a positive correlation with Δ SS especially towards the end of the core, from 46-51cm. However there are points where *H. elegans* and Δ SS do not correlate suggesting that current strength is not the only controlling factor for this species.

H. elegans is an opportunistic species, and is also known as an indicator of poorer oligotrophic environments and lower levels of an organic food supply to the ocean floor (Abu-Zied et al., 2008).

***Triloculina frigida* (Lagoe, 1977)**

Triloculina frigida prefers lower shelf slope and rise sediments which are disturbed by bottom currents and turbidity flows. It may be that this species tolerates these transported sediments as they often contain high levels of shallow water organic matter which has been transported from the shelf (Osterman et al., 2009). *T. frigida* has also been found at depths below 3000m, where it can tolerate a decrease in organic carbon content and a lower oxygen content of the top most sediments of the sea floor (Mackensen et al., 1984).

Levels of *T. frigida* are low throughout the core, until 48cm, where it significantly increases. This coincides with a drop in *H. elegans*. This also correlates to a drop in Δ SS which may suggest a correlation with these species and current strength.

***Globobulimina sp.* (Cushman, 1927)**

Globobulimina sp. is a hyaline foraminifera that is found in low oxygen environments, towards the dysoxic-anoxic boundary. It is infaunal, with some species being found at up to 15cm depth within the sediment (Corliss, 1985; Gupta and Machain-Castillo, 1993).

For this study, Globobulimina sp. was identified to genus level rather species due to the similar nature of the species and the difficulty of identifying between them.

Figure 8: Percentage abundance of dominating benthic foraminifera species identified in sediment core HH13-103MC. The core has been divided into six assemblage zones (AZ1-6) for ease of description. Dashed red line s mark the boundaries between Late, Mid and Early Holocene.

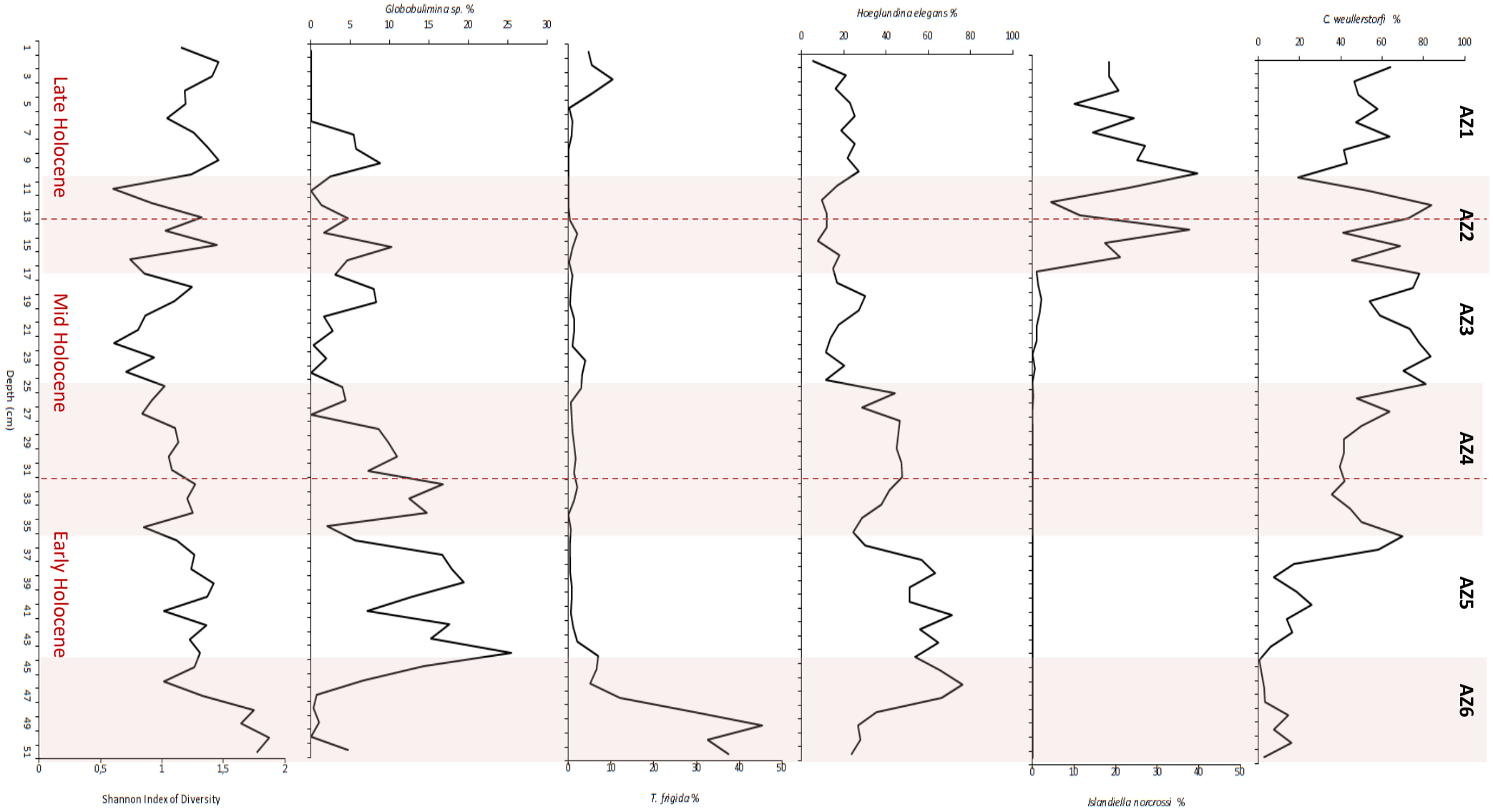

The benthic foraminifera found throughout core HH13-103MC can be divided into into six assemblage zones (AZ1-6). AZ1-3 show an overall increasing abundance of *C. wuellerstorfi*, and the highest abundances of *I. norcrossi*. AZ4-6 have an overall decrease of *C. wuellerstorfi*, and a significant increase of other dominating species; *H. elegans*, *T. frigida*, and *Globobulimina sp*.. *I. norcrossi* completely disappears from the sediment core in the later assemblage zones.

The identifications and characteristics of the individual assemblage zones are discussed below.

Assemblage Zone 1 (AZ1), 0-10cm

AZ1 is located at the top of the sediment core, from 0-10cm (0-3133Yrs BP). It is primarily dominated by *C. weullerstorfi*, however there is a general decreasing trend from 64% at the top of the assemblage zone to 19% at 10cm. This coincides with an increase of *I. norcrossi* of 18% at the top of the core to 39% at 10cm. however there are fluctuations with numbers decreasing at 4, 6 and 8cm. *H. elegans* also increases through AZ1, with the most significant abundance increase occurring at 0-2cm from 5% to 21% abundance. *T. frigida* and *Globobulimina sp*. have very low abundances throughout AZ1, of highs of 10% and 8% respectively.

Assemblage Zone 2 (AZ2), 10-16cm

The second assemblage zone identified is from 10-16cm, which dates at 3133-5351Yrs BP. The upper most boundary of AZ2 is identified by the significant increase of *C. wuellerstofi*, from 19-83% at 9-11cm depth. This negatively correlates with a significant decrease in *I. norcrossi*, from 39% reaching a low of 4% at 11cm. Overall AZ2 is dominated by *C. wuellerstorfi*, with levels of other species remaining low. *T. frigida* remains particularly low, averaging 0.7%, however a small peak of 2% occurs at 14cm (4990Ka BP) which occurs just before peaks of *H. elegans* and *Globobulimina sp*. at 15cm (5170Yrs BP) of 18% and 10% respectively. The lower end of AZ2 is identified though a significant decrease of *I. norcorss*i which drops from 21% at 15cm to 1% abundance at 16cm.

Assemblage Zone 3 (AZ3), 16-24cm

AZ3 ranges from 16-24cm depth within the sediment core, with and age range of 5351-6756Yrs BP. The main feature of this assemblage zone is the disappearance of *I. norcrossi*. Throughout AZ3 the abundance of *I. norcrossi* remains low, averaging 1%, however at the lower end of the assemblage zone it disappears altogether and does not recover, potentially signifying a climatic or environmental change. There is a small peak of *I. norcorssi* at 18cm (5712Yrs BP), which is also seen in several of the other benthic species, including *Globobulima sp*., *T. frigida*, and *H. elegans*. However this peak is not

reflected in the abundance of C. wuellerstorfi, rather at 18cm depth there is a decrease of abundance from 74% at 17cm down to 53%.

Assemblage Zone 4 (AZ4), 24-35cm

AZ4 is identified by a significant decrease of *C. wuellerstofi* at 24cm (6756Yrs BP) from 81% down to 47%. This declining trend continues throughout the assemblage zone, reaching a low of 35% at 32cm (8706Yrs BP). The decline of *C. wuellerstofi* occurs as other species increase in abundance, especially *H. elegans*, the abundance of which shows a direct negative correlation with *C. wuellerstorfi* throughout AZ4. Towards the bottom of the assemblage zone*, C. wuellerstorfi* starts to increase again, peaking at the bottom boundary of 35cm (9371Yrs BP) with an abundance of 69%. This dominance has an impact on the diversity of the assemblage, reducing H to 0.85. It also corresponds to a significant reduction of *Globobulimina sp*., down to 2% at 35cm.

Assemblage Zone 5 (AZ5), 35-44cm

The upper boundary of AZ5 is identified by a large decline of *C. wuellerstofi*, while *H. elegans* and *Globobulimina sp*. both show an increase of abundance. *C. wuellerstofi* reaches a low of 7% at 38cm (9629Yrs BP), while *H. elegans* increases to 63%, and *Globobulimina sp*. is at a high of 18% at the same sample depth. This negative correlation continues as *C. wuellerstorfi* peaks in the middle of the assemblage zone at 40cm (9800Yrs BP) with an abundance of 25%. Both *H. elegans* and *Globobulimina sp*. decrease at 40cm, with abundances of 51% and 12% respectively. The lower boundary of AZ5 is marked by the lowest abundance of *C. wuellerstorfi* seen throughout the sediment core, of 0.5% at 44cm (10144Yrs BP). This also corresponds to a high abundance of *Globobulimia sp*., reaching 25% at the same depth.

Assemblage Zone 6 (AZ6), 44-51cm

The bottom most assemblage zone, AZ4 dates from 10144-11585.5Yrs BP, and has a significantly different assemblage to those found at the top of the core. Here, *T. frigida* and *H. elegans* are the dominating species, with averages of 22% and 47% respectively. At 49cm (11135Yrs BP) *T. frigida* peaks at 48%, while the other species see a decrease at this point. *C. wuellerstorfi* remains low throughout AZ6, with two peaks at 48cm and 50cm. The peak at 50cm (11361Yrs BP) is also seen as small peak of *H. elegans*, however both *T. frigida* and *Globobulimin*a sp. show decreased abundances at this sample depth.

5.2.2 HH12-1206BC

A total of 31 species of benthic foraminifera were identified from the sediment samples of core HH12-1206BC, within the size fraction 100-500µm. The dominating species of benthic foraminifera found in core HH12-1206BC are discussed below.

***Cibicidoides weullerstorfi* (Schwager, 1866)**

For species description see section 5.2.1

***Islandiella norcrossi* (Cushman, 1933)**

For species description see section 5.2.1

***Hoeglundina elegans* (d'Orbigny, 1826)**

For species description see section 5.2.1

Reophax nodulosus (Brady, 1879)

R, nodulosus is and agglutinated species, which is found at depths from 73-4700m, with its habitat determined by the presence of cold bottom waters, meaning that it is a heterobathyl species (Llano and Wallen, 1971).

It has also been suggested that this species is an early colonizer of sediments transported by turbidites, and reworked sediments (Osterman et al., 2009).

Valvulineria arctica (Green, 1960)

V. arctica is an indicator species of shelf slope environments, preferring depths of 600-1000m, of temperatures ranging from 0.03 to -0.2^{o}C (Green, 1960).

***Cassidulina teretis* (Tappan, 1951)**

Cassidulina teretis in modern day assemblages prefers cold water masses and a fine grained sediment of organic rich mud. It is an indicator species of glaciomarine paleoenvironments (Mackensen and Hald, 1988).

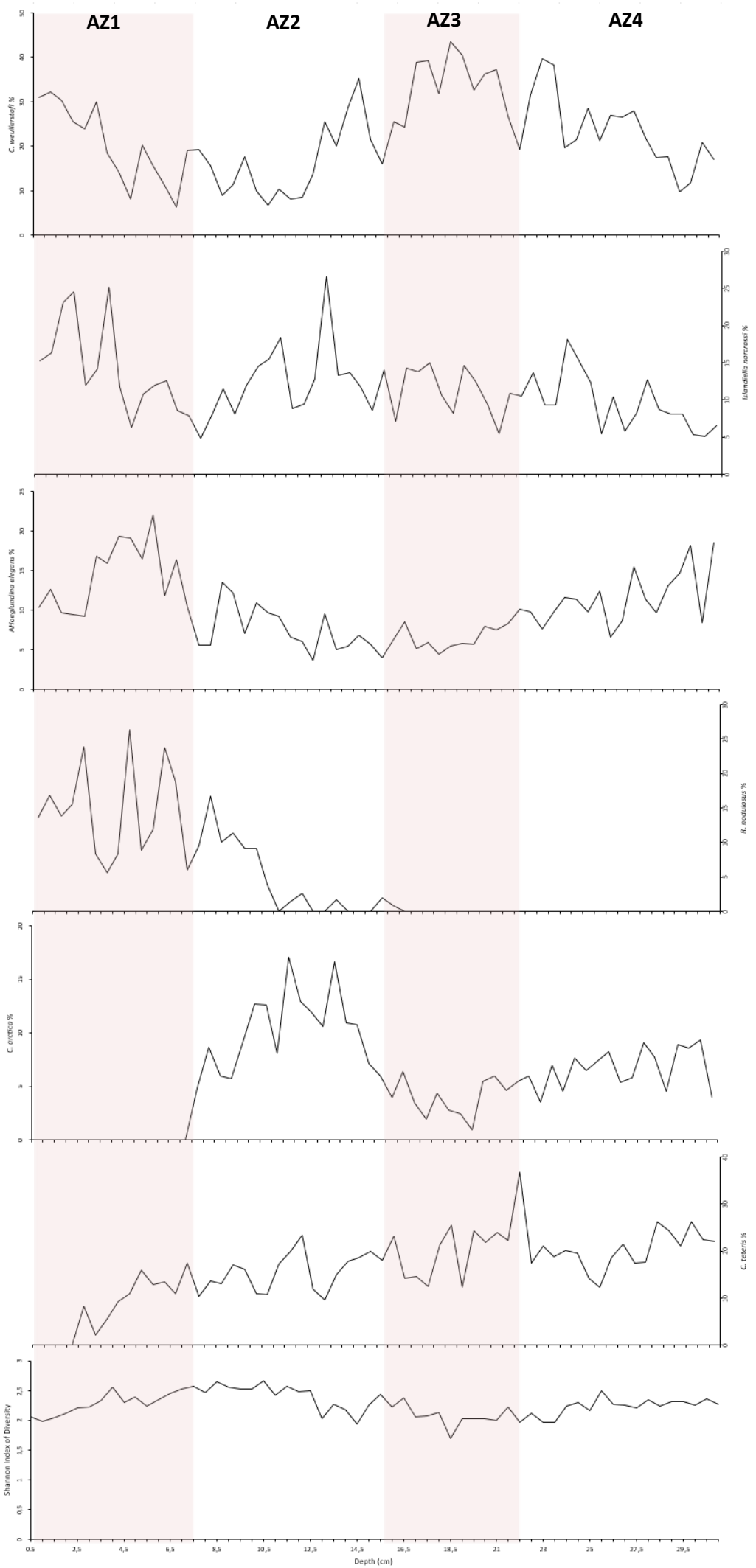

Figure 9: Calculated percentage abundances of the dominating benthic foraminifera identified in sediment core HH12-1206BC. Four assemblage zones were identified (AZ1-4).

Assemblage Zone 1 (AZ1), 0-7.5cm

AZ1 has been identified from 0-7.5cm depth (-62-339Yrs BP). It is characterised by an overall decreasing abundance of four of the dominant species; *C. wuellerstorfi*, *I. norcrossi*, *H. elegans* and *R. nodulosus*. Its lower boundary is defined by low abundances of *I. norcrossi* at 4.8%, *H. elegans* at 5.6%, and *R. nodulosa* at 6%. The lower boundary of AZ1 is also identified by the first appearance of *V. arctica* with an abundance of 4.8%.

Assemblage Zone 2 (AZ2), 7.5-16cm

The second assemblage zone identified has a depth range from 7.5-16cm (339-608Yrs BP). The upper boundary is identified by the first occurrence of *V. arctica*.

The most prominent feature of AZ2 is a peak of *I. norcorssi*, of 26.5% at 13cm depth (1390Yrs BP). This peak is also seen in *C. wuellerstorfi* and *H. elegans* with peaks of 12.5% and 9.5% respectively. However, *R. nodulosus, V. arctica* and *C. teretis* all show decreasing abundances at this sample depth. This increasing dominance of three species reduces the diversity of the assemblage, and H is seen to decrease at 13cm as the species evenness is reduced.

Throughout AZ2, abundances of *R. nodulosus* are significantly reduced compared to AZ1, with an average of 4% compared an average of 14% in AZ1.

Assemblage Zone 3 (AZ3), 16-22cm

AZ3 is identified at its upper boundary by the final occurrence of *R. nodulosus* within the core, with an abundance of 0.8%. In the same depth there is also a significant decrease of the abundance of *V. arctica*, at 4%. The abundance *V. arctica* remains low throughout the assemblage zone, with an average of 4%, reaching a low of 0.9% at 19.5cm. *H. elegans* and *I. norcrossi* are also low throughout AZ3, with averages of 6.5% and 11% respectively. These lows are in contrast to *C. wuellerstorfi*, which has the highest abundances during this assemblage, peaking at 18.5cm to 43.5%, and with an average of 33% for AZ3.

The lower boundary of AZ3 is identified by a significant decrease of *C. wuellerstorfi* of 19% at 22cm, while there is a large peak of *C. teretis* at the same depth, with an abundance of 36%.

Assemblage Zone 4 (AZ4), 22-31cm

The final assemblage zone identified in core HH12-1206BC is from 22-31cm, with an age range of 1105-1929Yrs BP.

This assemblage zone shows a negative correlation between *C. wuellerstofi* and *I. norcrossi*. At 23-23.5cm *C. wuellerstofi* shows a peak in abundance of 39-38%, while *I. norcrossi* has a low abundance at this depth, of 9%. *I. norcrossi* then increases rapidly to 18% abundance at 24cm, while *C. wuellersotfi* decreases to 19%. Therefore it is possible that these species have an inverse relationship. However, throughout AZ4 both *C. wuellerstorfi* and *I. norcrossi* show a decreasing trend of abundance, towards the end of the core.

This decrease trend is not found in *H. elegans*, which instead increases in abundance from 10% at 22cm to 18% at 31cm. *C. arctica* also shows an overall increasing abundance throughout this assemblage zone, from 5% at 22cm to 9% at 30.5cm. At 31cm it has decreased however to just 4% abundance.

At 26cm, there is low peak of abundance of *C. teretis* of 12%. This drop is also seen in *H. elegans* and *C. wuellerstorfi*, with abundances of 5% and 21% respectively. This drop in abundance does however increase diversity (H) of the assemblage, with H showing an increase to 2.5 at 26cm.

4.3 Carbon Dating and Age Model

4.3.1 HH12-1206BC

The AMS radiocarbon dating results are shown in Table 2 below. Four samples were chosen for testing, and dates have been correlated to allow for the Marine Reservoir Effect (R) and spatial correction (ΔR).

Lab number	Sample Depth (cm)	Midpoint of depth (cm)	Age 14C BP	Calibrated Years Before Present
Poz-57342	9,5-11,5	10,5	900 ± 80 BP	500
Poz-59605	19-20	19,5	1175 ± 30 BP	716
Poz-66211	23,5-25	24	1870 ± 70 BP	1716
Poz-57343	30-31	30,5	2320 ± 80 BP	1929

Table 2: AMS Radiocarbon dating results and calibrated ages for sediment core HH12-1206BC (Zamelczyk et al., in prep.)

The age model for these calibrated ages is shown below in Figure 10.

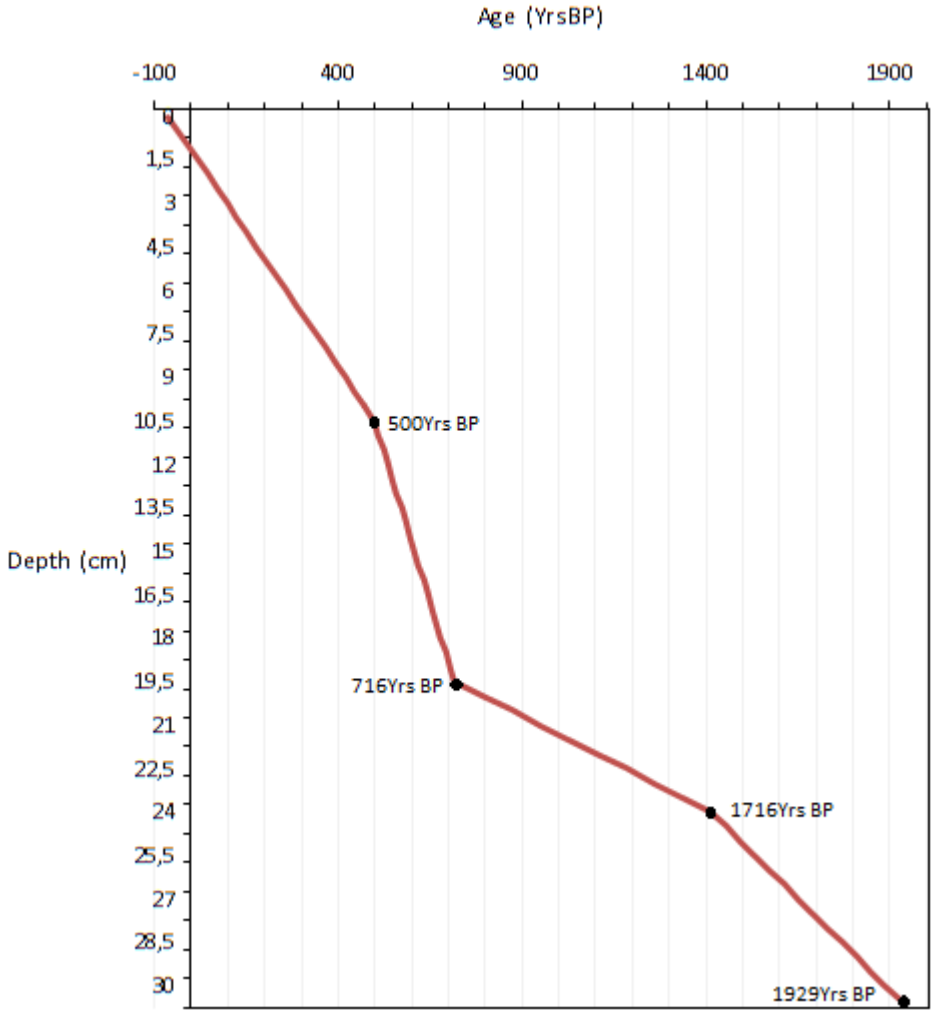

Figure 10: Calibrated carbon dated age model for sediment core HH12-1206BC. A linear rate of sedimentation was assumed between dated samples

To give ages to samples between AMS dates, a linear sedimentation rate (LSR) was calculated. This can be seen in Table 3 below.

Depth (cm)	Age 14C BP	Calibrated Years Before Present	LSR (cm/ka)	Yrs/cm
10.5	900 ± 80 BP	500	21	47.62
19.5	1175 ± 30BP	716	41.67	24.00
24	1870 ± 70 BP	1716	4.5	222.22
30.5	2320 ± 80 BP	1929	30.52	32.77

Table 3: Calculated LSR and Yrs/cm of sediment core HH12-1206BC. This was then used to date samples with unknown ages.

4.3.2 HH13-103MC

AMS radiocarbon dating for core HH13-103MC was unfortunately delayed at the time of writing, with only one sample returned. Therefore dating for this core was completed through calibration with core PS1243, taken from the east of the Jan Mayen Ridge at 2,700m depth. Due to the close nature of the sample sites it was possible to correlate the two cores. With one dated sample at 10-5cm for core HH13-103MC, a linear sedimentation rate was calculated between 0-10.5cm to determine the ages of the samples between these depths. Beyond this, sediment dates were correlated following the methods and data laid out by Bauch et al. (2001).

Lab Number	Sample Depth (cm)	Midpoint of depth (cm)	Age 14C BP	Calibrated Years Before Present
UBA-34979	10-11	10.5	3847	3447

Table 4: Single AMS Radiocarbon date for core HH13-103MC.

Using the calibration between the two cores, calibrated AMS radiocarbon dates were assigned to five further sample depths of core HH13-103MC. Using this data, the linear sedimentation rate (LSR) and the years per cm (yrs/cm). These values were then used to date samples between the known depth intervals. The age model for HH13-103MC can be seen in Figure 12.

Depth (cm)	Calibrated Years Before Present	LSR (cm/ka)	Yrs/cm
11	3447	3.19	313.36
14	4990	1.94	514.33
22	6435	5.54	180.63
30	7720	6.23	160.63
33	9200	2.03	493.33
45	10230	11.65	85.83

Table 5: Calculated LSR and Yrs/cm sedimentation rates for core HH13-103MC.

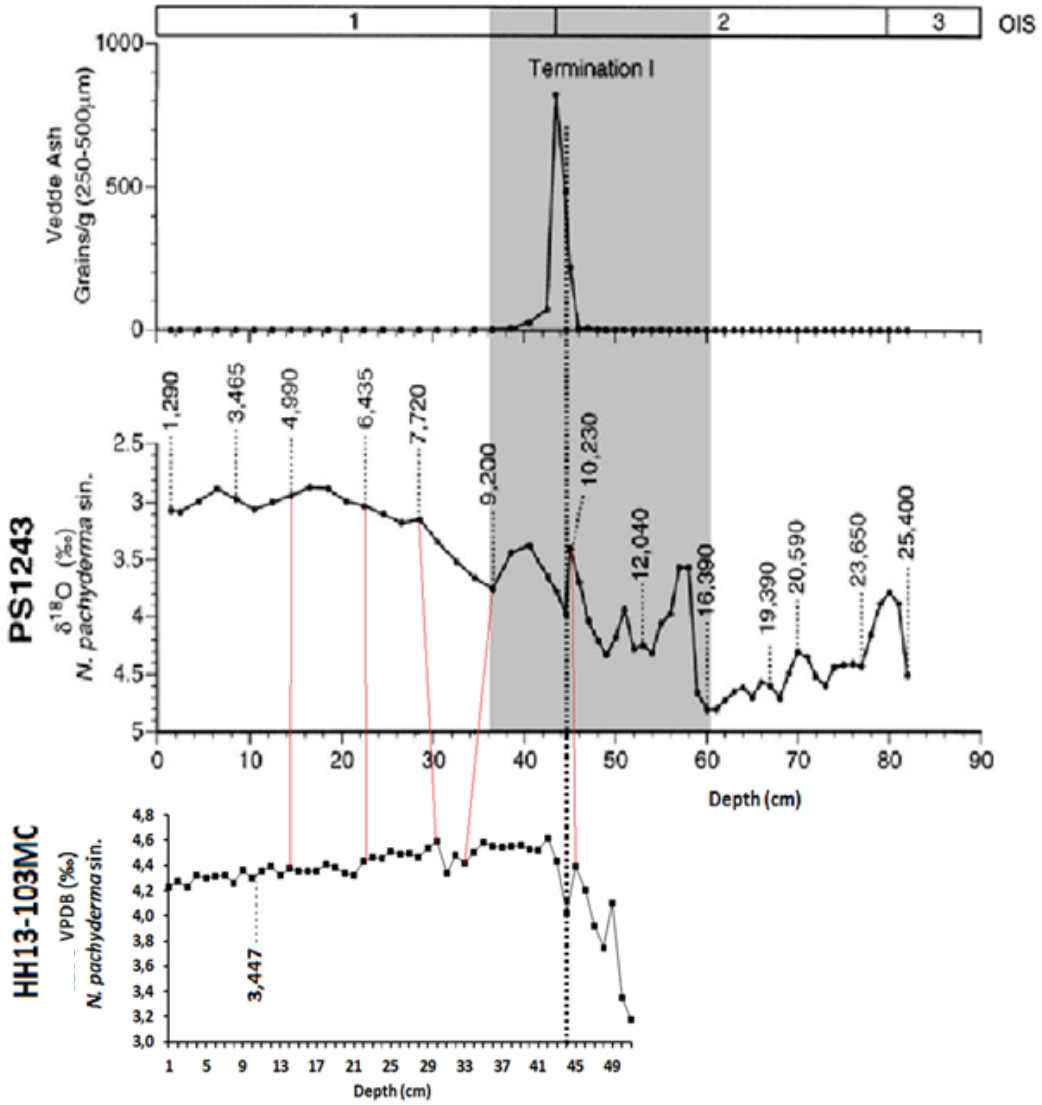

Figure **11** Correlation of cores HH13-103MC and PS1243 using δO^{18}‰ from *N. pachyderma* sinistral. Image adapted from Bauch et al., 2001. Dates are shown corrected for reservoir effect by subtracting 400yr.

Sedimentation rates and sample dates from 45-51cm were extrapolated using AMS Radiocarbon dates from core PS1243, assuming that core HH13-103MC followed the same trend of δO^{18} ‰ *N. pachyderma*. Correlation with core PS1243 is almost direct between samples depths, however there is some deviation with dates at 7,720 and 9,200YrsBP with differences in peaks of the δO^{18} found within this time period.

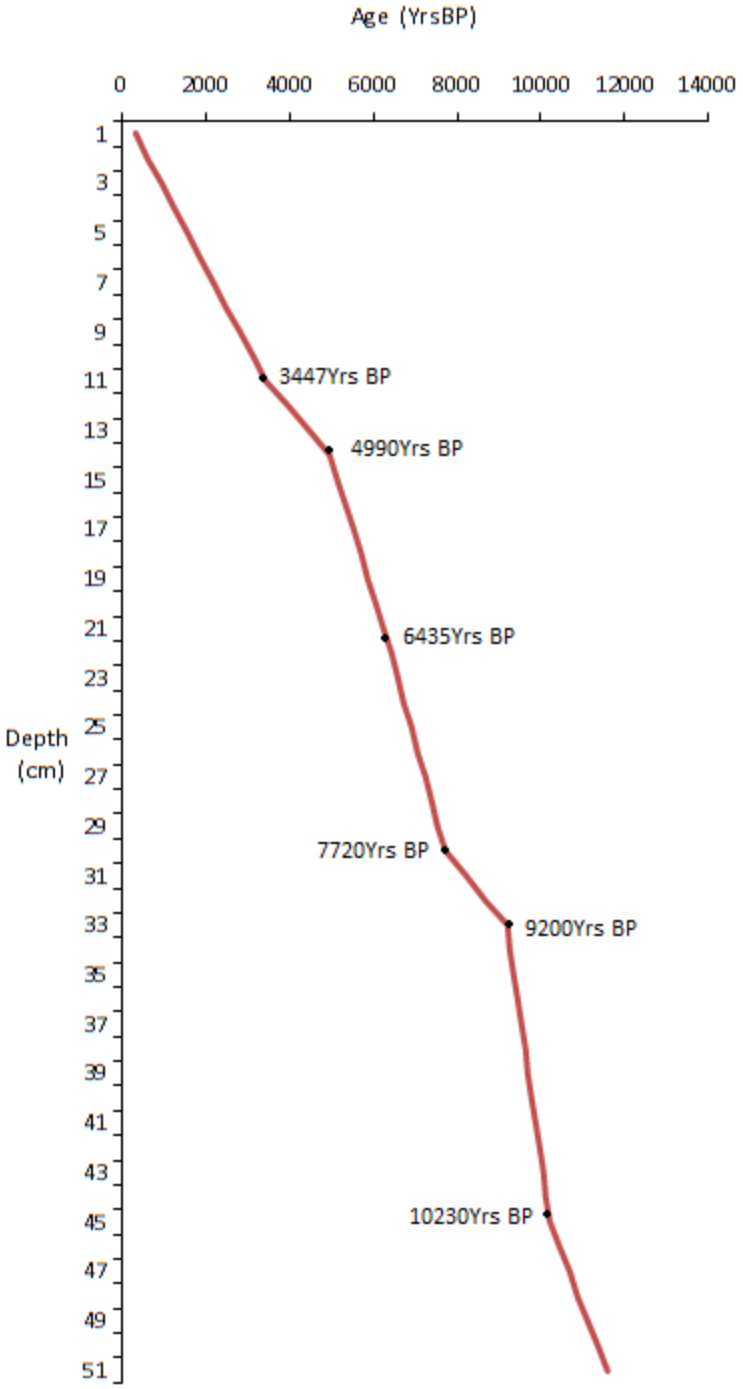

Figure 12: Age model of sediment core HH13-103MC. Dates were extrapolated using data from Bauch et al. (2001), and assuming a linear rate of sedimentation between dated sample depths.

4.4 Carbon and Oxygen Isotopes

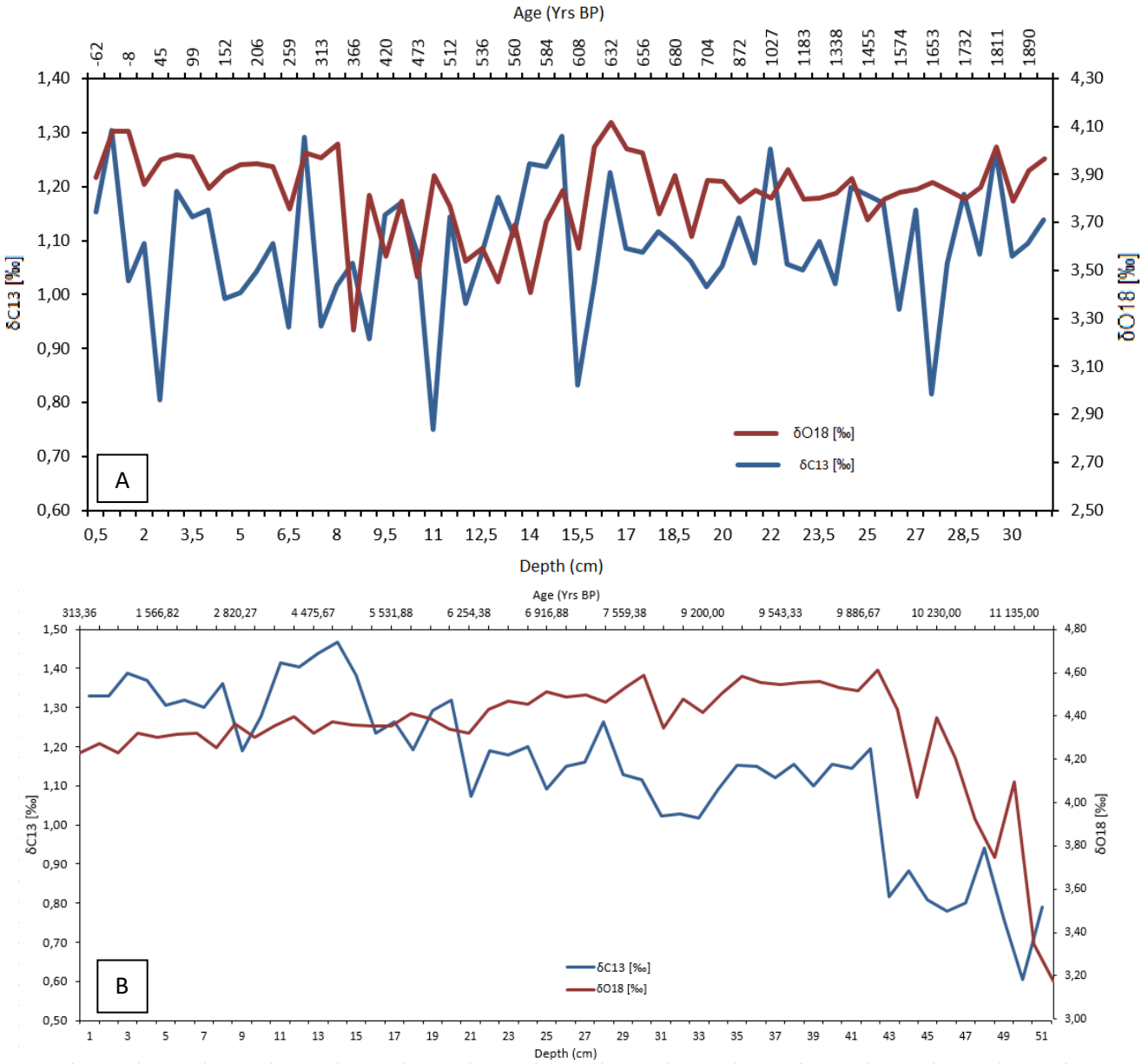

Figure 13: A) δO^{18} and δC^{13} (‰) records C. wuellerstorfi, collected from core HH12-1206BC. B) δO^{18} and δC^{13} (‰) records of C. wuellerstorfi collected from core HH13-103MC. Note the Axis differential between δO^{18} and δC^{13} on both graphs.

Oxygen and Carbon isotopes measured from the tests of C. wuellerstofi are shown in Figure 13, plotted against depth (cm) and depth (YrsBP). Correlation of the two sample sets can be seen in section 5.3.

4.4 Wet Bulk Density and Porosity

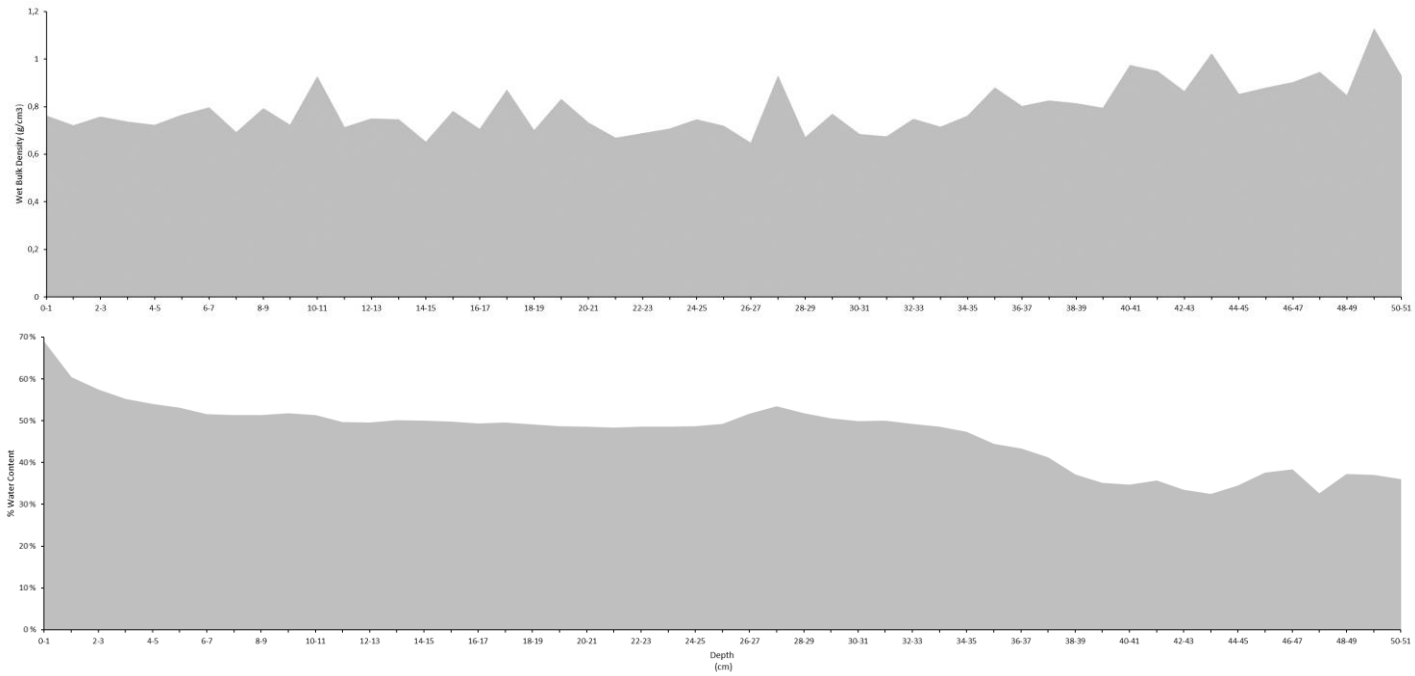

Figure 14: Calculated % water content and wet bulk density (g/cm^3) of sediment core HH13-103MC plotted against depth (cm).

Figure 14 shows the calculated percentage water content and wet bulk density (g/cm^3) (WBD) of sediment core HH13-103MC. The graphs show an inverse relationship between the two parameters, with wet bulk density increasing while % water content decreases. This is especially evident in the bottom half of the core, from 27-51cm. There are three large peaks of WBD, at 11, 27 and 50cm, with values of 0.72, 0.92 and 1.12g/cm^3 respectively.

5.5 Grain size analysis

Grain sizes of HH12-1206BC remain stable throughout the core, but there are noticeable peaks within the sand fraction at 21.5cm with a peak of 2.6%. There is also a large peak at 12cm of 2%. Towards the top of the core the percentage of sand increases dramatically, with the largest occurrence at 1cm with 5.2%.

Within core HH13-103MC, there is a large increase with the sand fraction seen from 32-43cm, with the greatest percentage seen at 39cm with 19%. Beyond this depth range, grain size remains stable throughout the core with only minor fluctuations. Noticeably there is an increase of sand at the bottom and top of the core, with peaks of 10% at 1cm and 18% at 51cm.

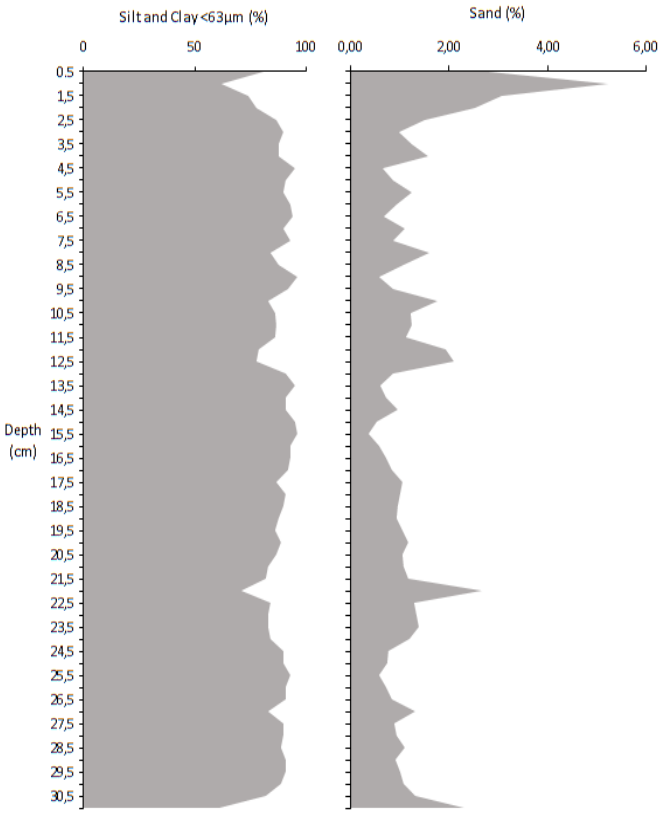

Figure 15: Grain size percentages collected for core HH12-1206BC (Zamelczyk et al., in prep,

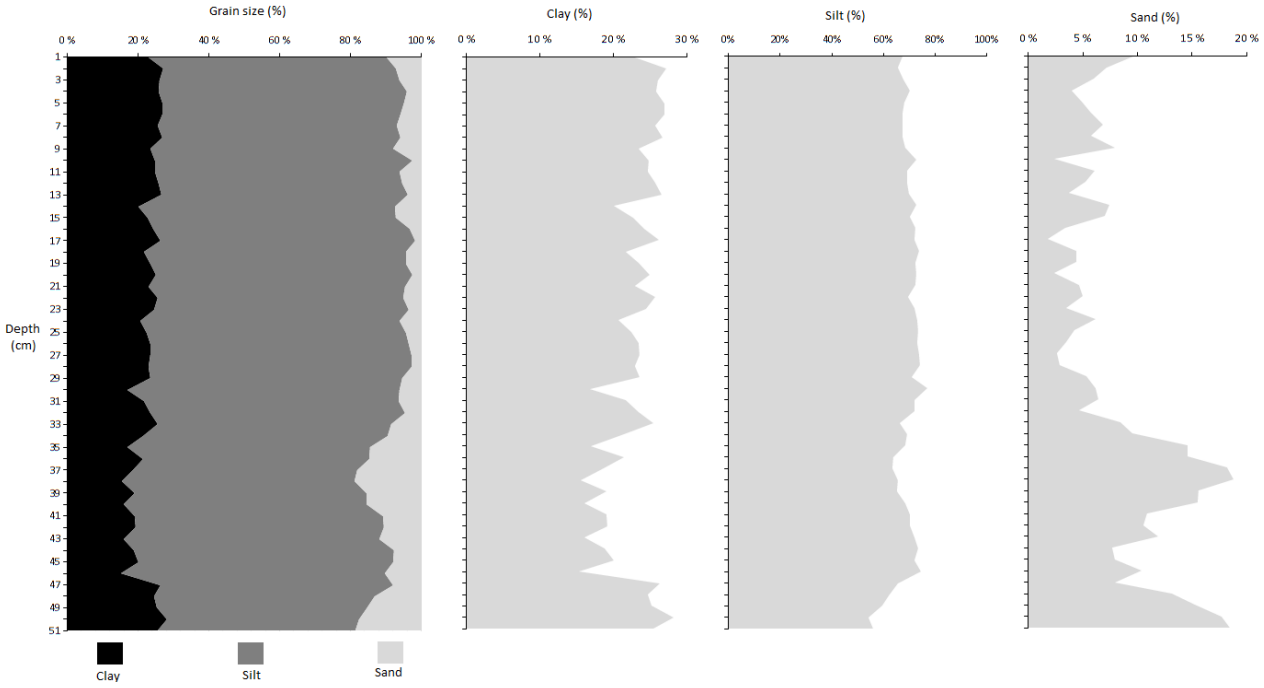

Figure 16: Grain sizes collected from core HH13-103MC. Sizes are presented separately and collectively to allow comparison of percentages.

5.6 Sortable Silt Analysis

From the grain size data collected, Sortable Silt (SS) was calculated and corrected for IRD. Higher positive values of corrected SS (ΔSS) indicate a stronger bottom water current while a decreased or negative value of ΔSS shows a reduced strength of bottom currents.

The SS_{pot} has a strong correlation with the percentage of sand grains found within the core, suggesting that the majority of sand sized particles are IRD, and have been transported to the core site via ice sheets/ice bergs. There are several periods of ΔSS decreasing while SS remains high, for example at 38, 24, and 14cm, which could indicate either cooling events with increased IRD flux or perhaps tephra layers.

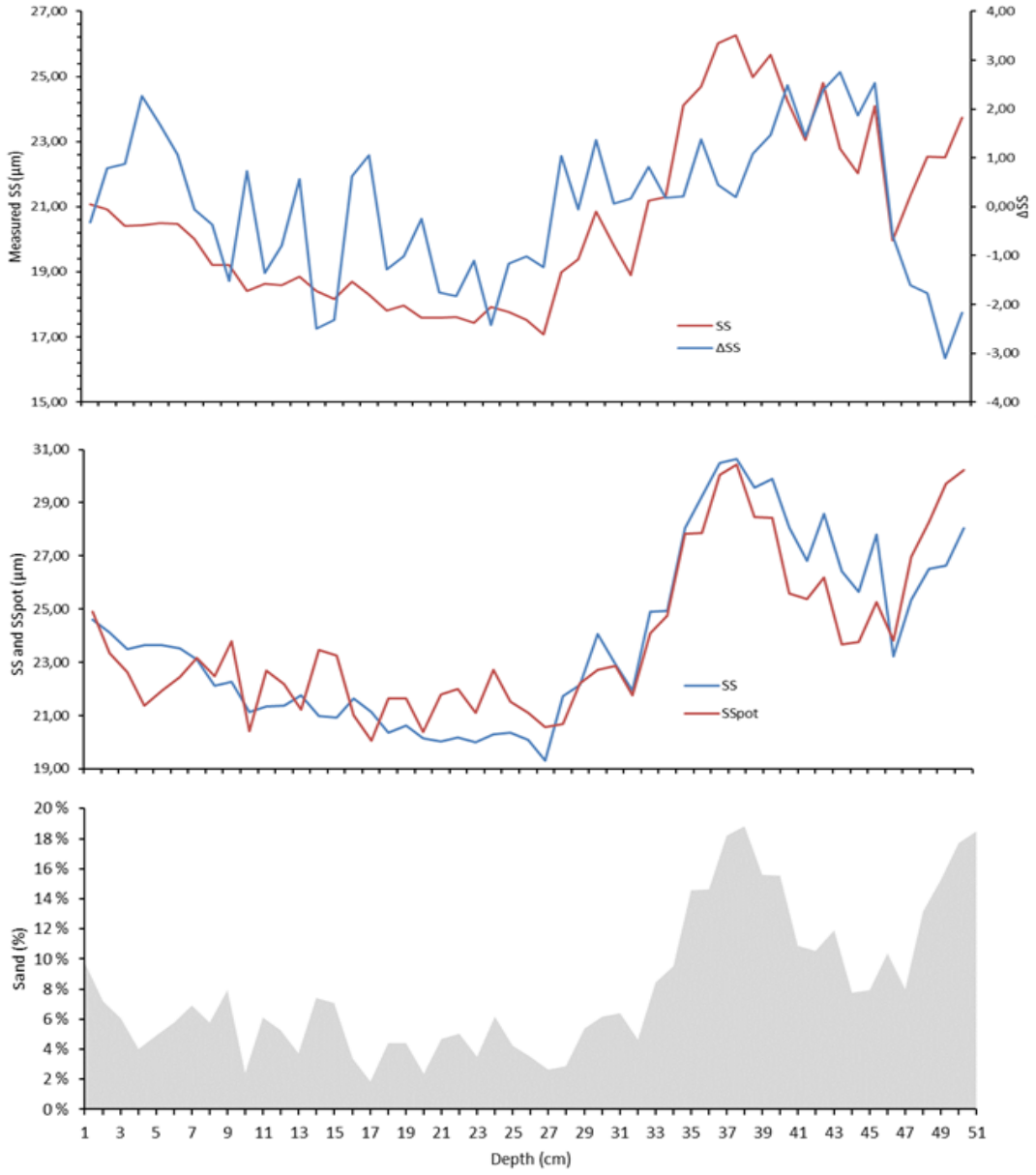

Figure 17: Results of sortable silts analysis for core HH13-103MC, showing ΔSS which has been corrected for possible sediment input from IRD. Sortable silt analysis was not conducted on core HH12-1206BC.

Chapter 5 - Discussion and Correlation of Cores

This section will interpret the results gathered during the study, and discuss their implications. At the start of this study it was thought to compare and contrast the two sediment cores, to build an understanding of how the Svalbard shelf and East Greenland paleoenvironments differed throughout the Holocene. However, after creating an age model for both cores this was no longer possible, given the different age ranges of the two cores. Therefore the cores will be discussed separately, with core HH12-1206BC providing a comparison only for the Late Holocene period. For ease of clarity, this section will first discuss sediment core HH13-103MC, for which the results have been divided into three sections by time period, to cover the Early, Mid, and Late Holocene. Further discussion will cover the results found in sediment core HH12-1206BC and the any comparisons between the core samples. Dates have been rounded to the nearest 100year for clarity.

5.1 The Early Holocene 11.5-8.2Ka BP

The Early Holocene is covered by the bottom of core HH13-103MC, from 51-31cm. It is dominated by *T. frigida* from 11.5-10.6Ka BP, with a peak of 49% at 11.1KaBP. This corresponds to a significant decrease of both δO^{18} and IRD Flux within the sediment, but a peak of δC^{13}. Lower levels of δO^{18} would suggest a warmer period, with lower IRD levels indicating reduced sea ice or icebergs. δC^{13} levels reach a small peak in this period, supporting an increase of surface productivity and water column ventilation. The low abundance of *H. elegans* and *Globobulimina sp*. with an increase of *T. frigida* would also support this, due to the preference of *H. elegans* and *Globobulimina sp*. for sediments with a low oxygen content. ΔSS is also low during this time, suggesting a lack of bottom currents or waning currents, and perhaps greater mixing of the water column.

These conditions are rapidly changed however from 10.6-10.4Ka BP. In the space of ~200yrs *T. frigida* has almost disappeared from the sediment, while *H. elegans* and *Globobulimina sp*. have increased significantly in abundance. This coincides with a large increase of δO^{18}, IRD flux and ΔSS, while δC^{13} remains relatively low. In a short time period conditions on the Jan Mayen ridge appear to have changed, with increased ice cover and/or icebergs, reducing productivity and the organic carbon content of the sea floor sediment which in turn created more favourable conditions for *H. elegans* and *Globobulimina sp.*

From 9.9-9.2Ka BP, levels of δO^{18} and δC^{13} remain relatively stable, however there are two large peaks of IRD flux at 9.9 and 9.4Ka BP. A previous peak of IRD at 10.2Ka BP can be attributed to the Vedde Ash (Bauch et al., 2001), so it is probable that these later peaks were also a result of volcanic eruptions.

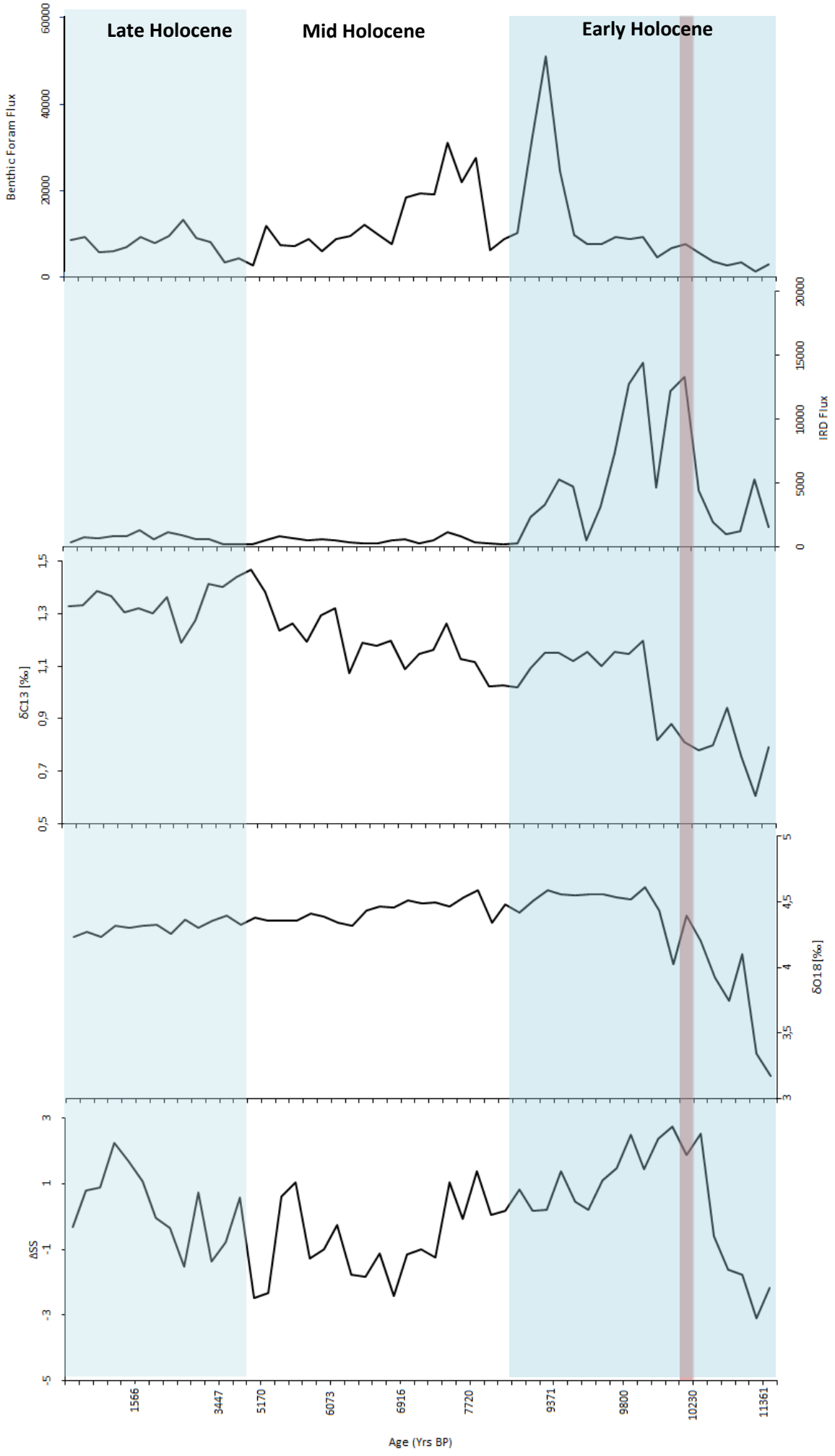

Figure 18: Data sets collected from HH13-103MC. ΔSS, δO^{18}, δC^{13}, IRD Flux and Benthic Foraminifera Flux. Shaded blue areas represent Late, Mid and Early Holocene, while the red line is known presence of Vedde Ash.

There is evidence from other locations with tephra dating to ~9.5Ka BP that there was a volcanic eruption at this time period (Pilcher et al., 2005), which would correlate with the peaks seen in the data collected. It is suggested by Davies et al. (2003) that the tephra layer occurring at this time originates from the Askja volcano located in Iceland.

Occurring at the same time as the latest large IRD flux peak, is a large rise of benthic foraminifera flux, from 9.2-9.4Ka BP. During this time, *C. wuellerstorfi* has an increased % abundance, while *H. elegans* and *Globobulimina sp*. are both low which would suggest an increase of oxygen levels within the sediment, and perhaps an increase of bottom current, although only a small increase of ΔSS is observed in this time period.

5.2 The Mid Holocene, 8.2-4.2Ka BP

A peak of δO^{18} at 8.2Ka BP suggests a short period of cooler temperatures, and this corresponds to cooling also seen in the GRIP ice cores (Alley et al., 1997) and marks the final phase of the Fennoscandian and Laurentide glaciations (Barber et al., 1999). It is thought that this cool period was caused by an increased flow of fresh melt water into the north Atlantic, thereby slowing the rate of production of North Atlantic Deep Water (NADW) (Rohling and Pälike, 2005). This decrease of NADW is reflected in a low abundance of *C. wuellerstorfi* at 8.2Ka BP.

The Mid Holocene is widely known for the Holocene Thermal Optimum, a period of warmer climatic conditions characterised by a period of higher summer temperatures throughout high latitudes of the Northern hemisphere, with higher summer insolation. The time scale of this period is not widely confirmed, but is generally determined to range from 9-4Ka BP (Kaufman et al., 2004; Renssen et al., 2009).

Overall, the data within the Mid Holocene shows a gradual decrease of δO^{18}, and a gradual increasing trend of δC^{13} which would suggest a general warming trend. One notable peak of δC13 during this time frame is found at 7.3Ka BP, which has a high benthic foraminifera flux, and smaller peaks of IRD flux, δC^{13} and ΔSS. These peaks could indicate a short period of increased mixing and stratification of the water column, possibly caused by an increasing bottom current strength. At the same time period there is a small decrease of δO^{18}, potentially reflecting a warmer climate. This may account for the increase of IRD flux, as warmer temperatures could lead to an increase of ice calving and ice melting. However, this is not greatly reflected in the benthic foraminifera assemblages, with abundances of *C. wuellerstorfi, H. elegans* and *T. frigida* remaining relatively constant. *Globobulimina sp*. on the other hand, drops significantly in abundance at this time, from 25% to 0%

within the period of ~160 years (7.3-7.2Ka BP). This could show an increase of oxygenation of sea floor sediments, supporting a greater level of mixing within the water column.

While there is an overall warming trend seen in the Mid Holocene, there are smaller peaks of colder climate conditions which correlate to data collected by Bond et al. (2001), using tracers within IRD as a proxy for sea ice cover. Colder periods suggested at 6.3 and 7.4Ka PB by these tracers match small peaks within the δO^{18} data of this study. The cooling events are also marked in the radiolarian record, occurring at ~7.2 and 6.4Ka BP (Dolven et al., 2002). These intervals correspond to increases of North Atlantic ice drift and can perhaps be correlated to other global events with colder and drier conditions and were potentially caused by the decreasing solar insolation throughout the Holocene, and possible periods of a slowing thermohaline circulation (Wanner et al., 2011). Low levels of ΔSS at these time periods are also noted in the data collected, and could indicate a reduced bottom current, along with a reduction of δC^{13} at 6.2Ka BP suggests an increased stratification of the water column, possibly due to an increase of ice cover.

The ~1000yrs of the Mid Holocene after the Holocene Thermal Maximum marks the start of the Neoglaciation which continued into the Late Holocene, from ~5.2-2Ka BP. The Neoglacial was a period of significant glacier advances in the Northern Hemisphere, with glacial moraines found across the world in high latitudes (Wanner et al., 2008). A significant decrease of ΔSS is seen in the data from 5.1-4.9Ka BP, which indicates a large decrease of bottom water current strength during this time period. δC^{13} is seen to peak at this time, to 1.45 ‰, the highest levels of δC^{13} seen throughout the whole sediment core. IRD flux and benthic flux levels however are minimal, with levels dropping between 5.1-3.9Ka BP. Both *H. elegans* and *C. wuellerstorfi* have a reduced abundance at this time, while *T. frigida* and *Globobulimina sp*. show small peaks, suggesting a low oxygen content, given the preferred environments of these species. The large increase of abundance of *I. norcrossi* between 5.1-4.9Ka BP and low benthic flux, shows higher levels of sea ice, or a closer proximity to sea ice, supporting these dates for potential growth of the Greenland ice sheet.

5.3 The Late Holocene, 4.2Ka PB to Present

The Neoglaciation continues from the Mid Holocene in to the Late Holocene. A continued decreasing trend of δO^{18} is seen throughout this time period, indicating warming to present day temperatures.

Within the foraminiferal assemblages, there is a large and sudden peak of *C. wuellerstorfi*, and decease of *I. norcrossi* abundances, from 3.4-3.9Ka BP. These changes occur at the same time that a decrease of ΔSS is observed in the sediment data. However, δO^{18} remains fairly constant at this time with only a small increase, and while δC^{13} is high, it is showing a decreasing trend from its previous

peak at 4.9Ka BP. This may indicate a “mini inter-glacial” period within the Neoglacial, indicating a retreat of the ice sheets. As the bottom current appears reduced at this time, perhaps there is a lag of organic carbon reaching the sea floor.

5.3.1 2000Yrs-Present

For the earliest Holocene to present it is possible to use data from both sediment cores, and compare spatially how the paleoclimate developed across the Nordic Sea. Five significant climatic events have been identified from the isotope data collected from *C. wuellerstorfi* sampled in core HH12-1206BC and are discussed below.

5.3.1.1 1653Yrs BP

The first climatic event that is identified in the very Late Holocene occurs at 1653Yrs BP, and sees a large decrease of δC^{13}, with a value of 0.82‰. This corresponds to peaks in % abundance of *H. elegans*, *C. teretis* and *I. norcrossi* in core HH12-1206BC, while *C. wuellerstorfi* has a small peak during this time in core HH13-103MC. *Globobulimina* sp. disappears completely at this time from core HH13-103MC suggesting a higher oxygen content of the sediment from this time to present. However this contrasts to the peaks of *H. elegans* and *C. teretis* found in core HH12-1206BC. The δC^{13} levels measured in core HH13-103MC are also seen to increase during this time, contradicting the values seen in HH12-1206BC. Therefore it is possible that the Svalbard shelf experienced a period of cooling, with lower oxygen levels and organic carbon content of the sediment, and increased ice cover due to the peaks of the above benthic species, while sediments further south in core HH13-103MC remained stable, with perhaps a small increase of NADW seen by increasing ΔSS and abundance of *C. wuellerstorfi*.

This cooling period corresponds to the Dark Ages Cold Period (DACP) from 400-800AD which would occur at ~1500-1100Yrs BP in the core. The DACP is due to a reduction of Atlantic Water (AW) and a stronger influence of Arctic Waters across the Arctic Front. (Mayewski et al., 2004; Spielhagen et al., 2011) The cold period found in the isotope record of this study is slightly earlier than found in other records which may be due to bioturbation or turbidity currents on the shelf slope reworking the sediment records.

5.3.1.2 632-608Yrs BP

The second climatic event identified occurs between 632-608Yrs BP, with a large decrease of both δC^{13} and δO^{18} across this time period in core HH12-1206BC. A peak of δO^{18} occurring just before at 632Yrs BP can be correlated across to δO^{18} values in HH13-103MC which also shows a peak at this

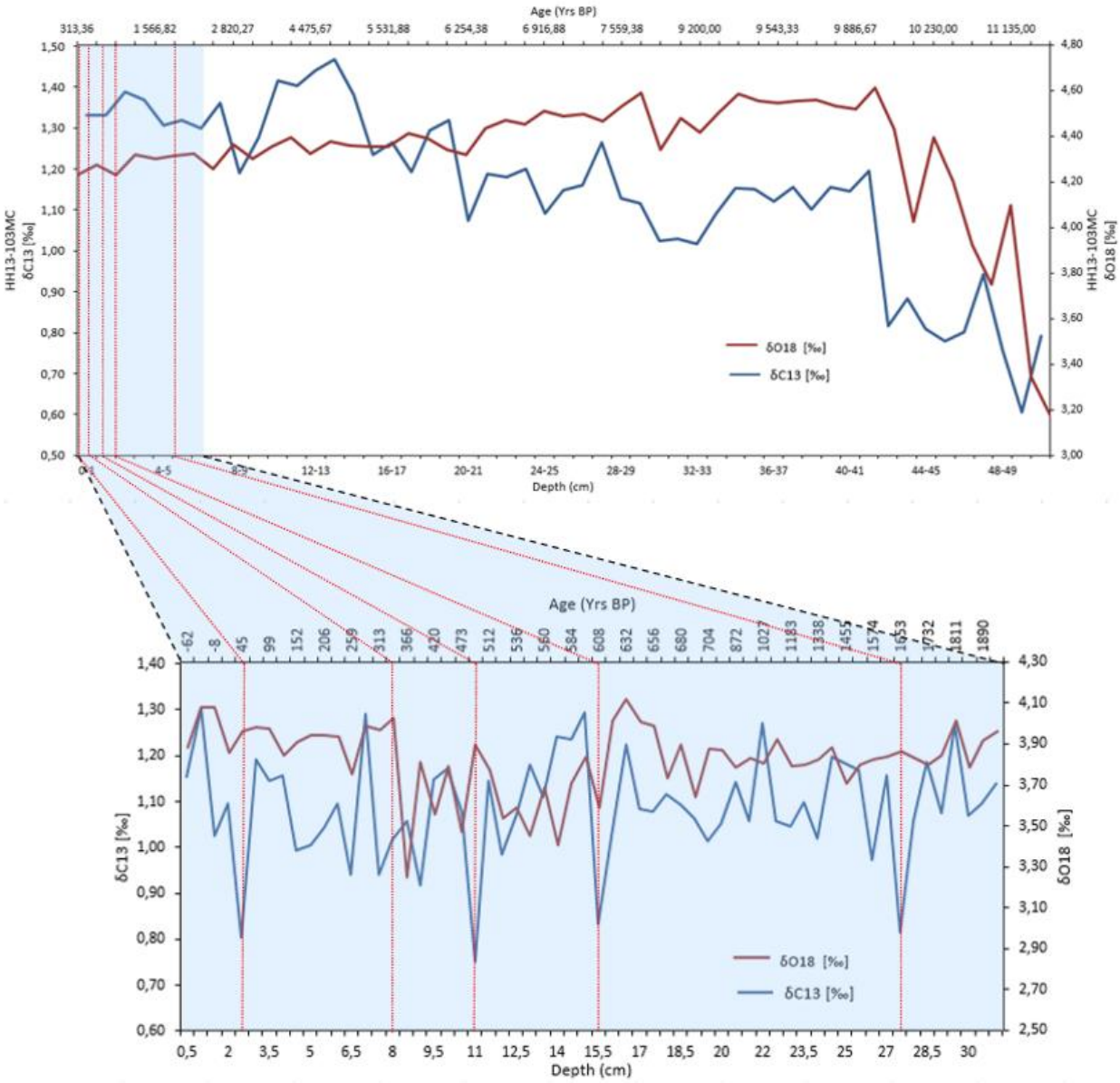

Figure 19: Temporal correlation of δO18 and δC14 records from C. wuellerstorfi collected in sediment cores HH13-103MC and HH12-1206BC. Red lines mark significant climatic events within the record.

time, suggesting a wide spread but short lived period of cooling, followed by a rapid period of warming. This could indicate the start of the Little Ice Age. Commencing at ~800Yrs BP, this was a period of cooling within the Holocene, with increased precipitation and advances of glaciers on Svalbard (Martin-Moreno, Alvarez and Hagen, 2017). From 872Yrs BP there is a general increasing trend seen in HH12-1206BC of δO^{18}, reaching a peak at 632Yrs BP, indicating a gradual cooling trend towards the Little Ice Age. However, it does not last long, with levels of δO^{18} dropping very quickly again from 620Yrs BP.

An increased abundance of I. norcrossi from 680-632Yrs BP could indicate a greater presence of sea ice, of the advancing proximity of the ice sheet. However these values are not stable and fluctuate between 7-15% abundance, suggesting a period of unstable climate. From 872Yrs BP *C. arctica* also sees a general increasing trend of abundance, peaking at 572Yrs BP with 16.7%. This increase could follow the advance of the DACP, as this species prefers temperatures of -0.2^{o}C.

Within core HH13-103BC, an increase of δO^{18} can be seen in the time period of ~8-600Yrs BP, meaning that the start of the Little Ice Age also effected temperatures further south on the Jan Mayen Ridge, perhaps with an colder inflow of the EGC becoming stronger at this time.

5.3.1.3 500Yrs BP

At 500Yrs BP, there is a peak of δO^{18} of 3.9‰, suggesting a short colder period. Coupled with extremely low values of δC^{13} of 0.75‰. At this time low abundances of *C. wuellerstorfi* are apparent, with a peak of *I. norcrossi*, supporting a colder time period with a closer proximity to the sea ice edge. It is suggested that this data represents the end of the LIA, as the trend seen in the record after this time is generally that of warming. Dates of the LIA are varied within the literature, and so it is possible that the cooling trend continued further than previous thought in this location due to its high latitude positon. Reconstructions by Kinnard et al. (2011) supports this, and also suggests temporary short periods of warming within the LIA which would match the isotope records of this study. Decreasing δO^{18} at 548 and 668Yrs BP could indicate responses to the advection of AW into the arctic on a decade scale as well as a centennial scale.

5.3.1.4 366-339Yrs BP

At this time period, a sharp increase of δO^{18} is observed, preceding this is a low level of δO^{18}, with climatic turn around occurring within a ~300 year time span. Changes are also observed within the foraminifera abundances, with lows of H*. elegans*, *R. nodulosus* and *I. norcrossi*. There is a dramatic change also of *C. arctica*, which within ~500 years, from 366-313YrsBP disappears completely from the sediment record. As an indicator species of colder water temperatures, the disappearance of *C. arctic* would point to warmer sea bed conditions. However this is in direct contrast to the large increase of oxygen isotopes at this time. It is possible that there is a lag in the response of *C. arctica*, which is effected by the decreasing levels of δO^{18} from 399-366Yrs BP.

5.3.1.5 45Yrs BP

At 45Yrs BP there is a fourth large decline of δC^{13} found within the isotope record. This decline is not visible within core HH13-103MC due to the reduced sedimentation rate of HH13-103MC. Therefore

it is not possible to correlate this event with environmental conditions further south in core HH13-103MC. This event is seen in the foraminifera record as a disappearance of *C. teretis*, and low abundances of *H. elegans*, *I. norcrossi* and *C. wuellerstorfi*. *R. nodulosus* however shows a large peak of abundance, reaching 23.8%. *R. nodulosus* is an agglutinated species of foraminifera, and this important distinction between the species could explain the differences in percentage abundances observed in the assemblage record; carbonate dissolution. The dissolution in this area is most likely caused by the presence of cold saline bottom waters. A high level of organic carbon production during spring and summer, combined with brine production during the formation increases the concentration of CO_2 in the surface waters, which is then transported downwards with the brines as they are denser than surrounding water masses. Sea ice cover would also restrict gas exchanges with the atmosphere, leading to the formation of a sink for atmospheric CO_2 (Steinsund and Hald, 1993; Murray and Alve, 1998).

Overall, core HH12-1206BC has a much higher rate of agglutinated foraminifera in comparison to HH13-103MC, which could be due to the different positions of the core locations. However it is difficult to make a true comparison due to the different age ranges of the two cores.

Chapter 6 - Conclusion

Correlation of two sediment cores of distinctly different ages and locations was attempted to be able to reconstruct paleoclimate and palaeoceanography of the Nordic Seas throughout the Holocene. This was met with limited success, due to the large differences of sedimentation rate found between the sample cores.

Core HH13-103MC spans nearly the whole Holocene time period, from 0-11.5KaBP. Through the Early Holocene (11.5-8.2KaBP) temperatures are unstable. Fluctuating δO^{18} and δC^{13} from 11.5-10.6Ka shows an overall decrease of temperature, matched by the benthic foraminiferal record with low abundances of *C. wuellerstorfi* and high abundances of *Globobulimina sp*. and *H. elegans*. Large peaks of IRD flux are apparent, which are seen as tephra layers within the core and match known volcanic eruptions such as the Vedde Ash layer at 10.2KaBP. A strongly positive ΔSS correlates to cooling temperatures and decreased mixing of the water column inferring strong bottom currents.

The Mid Holocene is relatively stable, with low abundances of *C. wuellerstorfi* indicating the 8.2KaBP cooling period, before the Holocene Thermal Maximum can be seen reflected in the decrease of the cold loving species *Globobulimina sp*.. Towards the end of the Mid Holocene increasing abundancy of I. norcrossi implies the start of the Neoglacial period, with periods of advancing glaciers and/or sea ice.

Increased warming continues throughout the Late Holocene, with stable levels of IRD and Benthic Flux. Decreasing *I. norcrossi* suggests that the ice front is pushed further north.

From 2KaBP attempts have been made to correlate both sediment cores to achieve a spatial idea of changing palaeoceanography. Two separate dates can be correlated across the cores, ~1.6KaBP and ~600YrsBP, with both sharing low levels of δC^{13}, suggesting poor levels of stratification in the water column across the Nordic Seas. Both of these dates can be attributed to the Dark Ages Cold Period.

Correlations after these dates becomes more difficult due to the different rates of sedimentation, 47Yrs/cm and 313Yrs/cm for HH12-1206BC and HH13-103MC respectively.

Therefore reconstruction of the Late Holocene is primarily made through interpretations of sediment core HH12-1206BC. From 45YrsBP to Present isotope levels can be seen reaching the Modern Maximum, suggesting that water masses have changed in the last ~100Yrs with increasing temperatures. Although it is not known for sure if this rise of temperature is a product of changing water masses of increased warm AW advection or due to anthropological influences.

Chapter 7 - Future Work

While work has been completed on both of the cores discussed in this study, there are multiple options of how work could continue to gain further insight. While both Oxygen and Carbon isotopes have been measured there is possibility for temperature reconstructions using transfer functions, would give a much deeper insight into the changing bottom water conditions, and if these had an impact on the benthic foraminifera assemblage.

There was also a great difficulty obtaining AMS dates for core HH13-103MC, which has severely decreased the accuracy of this study. With time, dates for this core could be collected and applied to give a more accurate correlation of the two cores, and allow a greater context to the other data collected for HH13-103MC.

Due to previous studies in the area and ongoing projects at the time of writing, tephra layers were not included in this study, except for dating purposes. This could be another point of interest for core HH13-103MC given its close proximity to both Jan Mayen and Iceland.

Further data to be collected would be the Total Organic Carbon (TOC). While it was not sampled for this study, samples collected from core HH13-103MC are still available for this purpose and would add to further studies. Samples are also available for the collection and study of planktic foraminifera.

References

Aagaard K., Swift J., Carmack E., 1985, Thermohaline Circulation in the Arctic Mediterranean Seas, Journal of Geophysical Research, Vol. 90, pp. 4833-4846

Aagaard-Sørensen et al., 2013, Sub Sea surface temperatures in the Polar North Atlantic during the Holocene: Planktic foraminiferal Mg/Ca temperature reconstructions, *The Holocene*, Vol. 24, Issue 1, pp. 93 – 103

Abu-Zied R., Rohling E., Jorissen F., Fontanier C., Casford J. and Cooke S., 2008, Benthic foraminiferal response to changes in bottom-water oxygenation and organic carbon flux in the eastern Mediterranean during LGM to Recent times, *Marine Micropaleontology*, Vol. 67, pp. 46-68

Alley, R., Mayewski, P.A., Sowers, T., Stuiver, M., Taylor, K.C., Clark, P.U., 1997. Holocene climatic instability: a prominent, widespread event 8200 yr ago. *Geology*, Vol. 25, pp. 483-486

Alve, E., and Bernhard, J.M., 1995, Vertical migratory response of benthic foraminifera to controlled oxygen concentrations in an experimental mesocosm, *Marine Ecology Progress Series*, Vol. 116, pp. 137-151.

Andersen C., Koc N., Jennings A., Andrews J.T., 2004, Non-uniform response of the major surface currents in the Nordic Seas to insolation forcing: implications for the Holocene climate variability, *Paleoceanography*, Vol. 19, PA000873.

Andersson C., Pausata F. S. R., Jansen E., Risebrobakken B., and Telford R. J., 2010, Holocene trends in the foraminifer record from the Norwegian Sea and the North Atlantic Ocean, *Climate of the Past*, Vol. 6, pp. 179–193

Ascough P., Cook G., and Dugmore A., 2005, Methodological approaches to determining the marine radiocarbon reservoir effect, *Progress in Physical Geography*, Vol. 29, pp. 532-547

Barber, D.C., Dyke, A., Hillaire-Marcel, C., Jennings, A.E., Andrews, J.T., Kerwin, M.W., Bilodeau, G., McNeely, R., Southon, J., Morehead, M.D., Gagnon, J.-M., 1999. Forcing of the cold event of 8,200 yearsago by catastrophicdrainage of Laurentidelakes, *Nature*, Vol. 400, pp. 344-348

Bauch H. et al., 2001, A multiproxy reconstruction of the evolution of deep and surface waters in the subarctic Nordic seas over the last 30,000 yr, *Quaternary Science Review*, Vol. 20, pp. 659-678

Brasier, M. D., 1980, Microfossils, George Allen & Unwin LTD, London, pp. 90-121

Bond et al., 2001, Persistent solar influence on the north Atlantic climate during the Holocene, *Science*, Vol. 294, pp. 2130-2136

Corliss, B.H., 1985, Microhabitats of benthic foraminifera within deep-sea sediments, *Nature*, Vol. 314, pp. 435-438

Davies, S. W., Wastegard, S. and Wohlfarth, B., 2003. Extending the limits of the Borrobol tephra to Scandinavia and detection of new Holocene tephras. *Quaternary Research*, Vol. 59, pp. 345–352

Dijkstra et al. (2013) Baseline benthic foraminiferal assemblages and habitat conditions in a sub-Artcic region of increasing petroleum development, *Marine Environmental Research*, Vol. 92, pp. 178-19

Dolven, J. K., Cortese G., and Bjørklund K., 2002, A high-resolution radiolarian-derived paleotemperature record for the Late Pleistocene-Holocene in the Norwegian Sea, *Paleoceanograpy*, Vol. 17(4), pp. 1-13

Duplessy et al., 2001, Holocene paleoceanography of the northern Barents Sea and variations of the northward heat transport by the Atlantic Ocean. *Boreas*, Vol. 30, pp. 2–16. Oslo. ISSN 0300-9483.

Fisher T.G., Smith D.G., and Andrews J.T., 2002, Preboreal oscillation caused by a glacial Lake Agassiz flood, *Quaternary Science Reviews*, Vol. 21, pp. 873–878.

Gjerløw E., Haflidason and Pederen, (2016) Holocene explosive volcanism of the Jan Mayen volcanic province, North-Atlantic. Journal of Volcanology and Geothermal Research, Vol. 321, pp. 31-43

Gooday A. J., 2003, Benthic foraminifera (Protista) as tools in deep-water palaeoceanography: Environmental influences on faunal characteristics, *Advances in Marine Biology*, Vol. 46, pp. 1-90

Gray, S., 2000, The measurement of marine species diversity, with an application to the benthic fauna of the Norwegian continental shelf, *Journal of Experimental Marine Biology and Ecology*, Vol. 250, pp. 23-49

Green K. E., 1960, Ecology of some Arctic Foraminifera, *Micropaleontology*, Vol. 6, pp. 57-78

Groot et al., 2014, Reconstruction of Atlantic water variability during the Holocene in the western Barents Sea, *Climate of the Past*, Vol. 10, pp. 51-62

Gupta B. K. and Machain-Castilla M., 1993, Benthic Foraminifera in oxygen poor habitats*, Marine Micropaleontology*, Vol. 20, pp. 183-201

Gupta B. K., 2007, Modern Foraminifera, Springer Science and Business Media. ISBN: 0306481049, 9780306481048

Hald M., Andersson C., Ebbesen H., Jansen E., Klitgaard-Kristensen D., Risebrobakken L., Salomonsen G. R., Sarnthein M., Sejrup H. P., and Telford R. J., 2007, Variations in temperature and extent of Atlantic Water in the northern North Atlantic during the Holocene, *Quaternary Sci. Rev*., Vol. 26, pp. 3423–3440

Hammer, Ø., Harper, D.A.T., Ryan, P.D. 2001. PAST: Paleontological statistics software package for education and data analysis. Palaeontologia Electronica 4(1): 9pp. http://palaeo-electronica.org/2001_1/past/issue1_01.htm

Hass, C. H., 2002. A method to reduce the influence of ice-rafted debris on a grain size record from northern ram straight, Arctic Ocean. *Polar research*, Vol. 21 (2), pp. 299-306.

Hofmann R., Can Foraminifera be used as indicator of environmental changes? Technische Universität Bergakademie Freiberg, http://www.geo.tufreiberg.de/oberseminar/os05_06/richard_hoffmann.pdf Accessed 2/10/2016

Husum, K., Hald, M., 2012, Arctic planktic foraminiferal assemblages: Implications for subsurface temperature reconstructions, *Marine Micropaleontology*, pp.96-97

Kaufman et al., 2004, Holocene thermal maximum in the western Arctic, *Quaternary Science Reviews*, Vol. 23, pp. 529-560

Jessen, S.P. and Rasmussen, T.L., 2015, Sortable silt cycles in Svalbard slope sediments 74–0 ka, *Journal of Quaternary Science*, Vol. 30(8), pp.743-753.

Kinnard et al., 2011, Reconstructed changes in Arctic sea ice over the past 1,450 years, Nature, Vol. 479, pp. 509-512

Korsun S., and Hald M., 2000, Seasonal Dynamics of Benthic Foraminifera in a Glacially Fed Fjord of Svalbard, European Arctic, *Journal of Foraminiferal Research*, Vol. 30, no. 4, pp. 251–271

Llano G. and Wallen I., 1971, Biology of the Antarctic Seas, Vol. 17, Americn Geophysical Union, USA, pp. 289-280

Loeblich, A. R. and Tappan, H., 1987. Foraminiferal Genera and their Classifiaction. New York: Van Nostrand Reinhold, vols. 1 and 2.

Lutz G. F. and Thiel H., 1989, Epibenthic Formainifera from elevated microhabitats: Cibicidoides wuellerstorfi and Planulina arminensis*, Journal of Foraminiferal Research*, Vol. 19, no. 2, pp. 153-158

Mackensen A. and Bickert T., 1999, Stable Carbon Isotopes in Benthic Foraminifera: Proxies for Deep and Bottom Water Circulation and New Production, *Use of Proxies in Paleoceanography: Examplesfrom the South Atlantic*. Springer-Verlag Berlin Heidelberg, Edited by Fischer G. and Wefer G., pp 229-254

Mackensen A. and Hald M., 1988, Cassidulina teretis and C. laevigata: Their modern and late quaternary distribution in Northern Seas, *Journal of Foraminiferal Research*, Vol. 18, pp. 16-24

Mackensen A., Sejrup H. and Jansen E., 1984, The Distribution of Living Benthic Foraminifera on the Continental Slope and Rise off Southwest Norway, *Marine Micropaleontology*, Vol. 9, pp. 275-306

Mann et al., 2009, Global signatures and Dynamical origins of the Little Ice Age and Medieval Climate Anomoly, *Science*, Vol. 326, pp. 1256-1260

Martin-Moreno R., Alvarez F. A., Hagen J. O., 2017, 'Little Ice Age' glacier extent and subsequent retreat in Svalbard archipelago, *The Holocene*, pp. 1-12

Mayewski et al., 2004, Holocene Climate Variability, *Quaternary Research*, Vol. 62, pp. 243-255

McCave I. N., Manighetti B. and Robinson S., Sortable silt and fine sediment size/composition slicing: Parameters for palaeocurrent speed and palaeoceanography, *Paleoceanography*, Vol. 10 (3), pp. 595-610

Meincke J., Rudels B., and Friedrich J., 1997, The Arctic Ocean-Nordic Seas thermohaline system, Journal of Marine Science, Vol. 54, pp. 283-299

Moros M., Andrews J. T., Eberl D. D., and Jansen E., 2006, Holocene history of drift ice in the northern North Atlantic: Evidence for different spatial and temporal modes, *Paleoceanography*, Vol. 21

Murray J. M. and Alve E., 1999, Natural dissolution of modern shallow water benthic foraminifera: taphonomic effects on the palaeoecological record, *Palaeogeography, Palaeoclimatology, Palaeoecology*, Vol. 146, pp. 195-209

Murray J. M., 2006, Ecology and Applications of Benthic Foraminifera, Cambridge University Press, New York, pp. 426–429

Osterman L, Poore R. and Foley K., 2009, Distribution of Benthic Foraminifers in the Surface Sediments of the Arctic Ocean, *U.S. Geological Survey Bulletin*, Vol. 2164, U.S Government Printing Office, University of Minnesota

Oilcher J., Bradley R., Francus P. and Anderson L., 2005, A Holocene tephra record from the Lofoften Islands, Arctic Norway, *Boreas*, Vol. 34, pp. 136-156

Rasmussen, T. L. et al., 2007. Paleoceanographic evolution of the SW Svalbard margin (76°N) since 20,000 14C yr BP. *Quaternary Research*, Vol. 67, pp. 100-114.

Rasmussen, T. L. et al., 2014. Spatial and temporal distribution of Holocene temperature maxima in the northern Nordic seas: interplay of Atlantic-, Arctic- and polar water masses. *Quaternary Science Reviews*, pp. 280-291.

Rasmussen T. L. and Thomsen E., 2014, Palaeoceanographic development in Storfjorden, Svalbard, during the deglaciation and Holocene: evidence from the benthic foraminiferal records, *Boreas*, Vol.44, pp. 24-44

Reimer et al., 2013. IntCal13 and Marine13 radiocarbon age calibration curves 0–50,000 year's cal BP. *Radiocarbon*, 55(4), 1869-1887.

Rensen et al., 2009, The spatial and temporal complexity of the Holocene thermal maximum, *Nature Geoscience*, Vol. 2, pp. 411-414

Risebrobakken et al., 2010, Climate and oceanographic variability in the SW Barents Sea during the Holocene, *The Holocene*, Vol. 20, pp. 609-621

Risebrobakken, B., Dokken, T., Smedsrud, L.H., Andersson, C., Jansen, E., Moros, M., Ivanova, E.V., 2011. Early Holocene temperature variability in the Nordic Seas: the role of oceanic heat advection versus changes in orbital forcing, *Paleoceanography*, Vol. 26, DOI: 10.1029/2011PA002130

Rohling E. and Pälike H., 2005. Centennial scale climate cooling with a sudden cold event around 8,200years ago, *Nature*, Vol. 434

Schneider A., 2015, Lecture on biological and geochemical proxies, UiT The Arctic University of Norway, Department of Earth Sciences.

Schepper et al., 2015, Early Pliocene onset of modern Nordic Seas circulation related to ocean gateway changes, *Nature Communications*, Vol. 6, DOI: 10.1038/ncomms9659

Shannon, C. E., 1948, A Mathematical Theory of Communication, *Bell System Technical Journal*, Vol. 27, pp. 379–423

Shimura T. et al., 2012, Variation in stable carbon and oxygen istotopes of individual benthic foraminifera: tracers for quantifying the magnitude of isotopic disequilibrium, *Biogeosciences*, Vol. 9, pp. 4353-4367

Spielhagen et al., 2011, Enhanced modern heat transfer to the Arctic by Warm Atlantic Water, *Science*, Vol. 331, pp. 450-453

Steinsund P. I. and Hald M., 1994, Recent calcium carbonate dissolution in the Barents Sea: Paleoceanographic applications, *Marine Geology*, Vol. 117, pp. 303-316

Udden, J.A., 1914, Mechanical composition of clastic sediments. *Bulletin of the Geological Society of America*, Vol. 25, pp. 655-744.

Walker, M., Berkelhammer, M., Björck, S., Cwynar, L., Fisher, D., Long, A., Lowe, J., Newnham, R., Rasmussen, S. and Weiss, H. (2012). Formal subdivision of the Holocene Series/Epoch: a Discussion Paper by a Working Group of INTIMATE (Integration of ice-core, marine and terrestrial records) and the Subcommission on Quaternary Stratigraphy (International Commission on Stratigraphy). *Journal of Quaternary Science*, Vol. 27, pp.649-659.

Wanner et al., 2008, Mid-Late Holocene climate change: an overview, *Quaternary Science Review*, pp. 1-38

Wanner H., Solomina O., Grosjean M., Ritz S., Jetaj M., 2011, Structure and origin of Holocene cold events, Quaternary Science Review, Vol. 30, pp. 3109-3123

Wentworth C.K., 1922, A scale of grade and class terms for clastic sediments. *Journal of Geology*, Vol. 30, pp. 377-392.

WoRMS Editorial Board, 2017, World Register of Marine Species. Available from http://www.marinespecies.org at VLIZ. Accessed 2017-07-16. doi:10.14284/170

Zamelczyk et al., in prep.